Kinematic Alignment of Precision Robotic Elements in Factory Environments

by

Patrick Willoughby

B. S. Mechanical Engineering
University of Pittsburgh, 20001

Submitted to the Department of Mechanical Engineering
in Partial Fulfillment of the Requirements for the Degree of

Master of Science in Mechanical Engineering
at the
Massachusetts Institute of Technology

January 2002

Signature of Author . . . .
Department of Mechanical Engineering
January 16, 2002

Certified by . . . .
Alexander H. Slocum
Professor of Mechanical Engineering
Thesis Supervisor

Accepted by . . . .
Ain Sonin
Chairman, Department Committee on Graduate Students

Kinematic Alignment of Precision Robotic Elements in Factory Environments

by

PATRICK WILLOUGHBY

Submitted to the Department of Mechanical Engineering
on January 18, 2002 in Partial Fulfillment of the
Requirements for the Degree of Master of Science in
Mechanical Engineering

ABSTRACT

In the measurement and instrumentation fields, kinematic couplings have been widely used to create precise and repeatable interfaces on a variety of devices. However, these devices have been limited to low load and clean environments such as in semiconductor manufacturing facilities. While traditional factory environments present less ideal conditions for the implementation of kinematic couplings, the benefits of more repeatable, deterministic interfaces is becoming more necessary as tolerances for products continue to become more stringent.

In this thesis, general exact constraint and kinematic coupling design theory is discussed with specific application for use in industrial environments. Factors such as installation and cleanliness are discussed along with traditional design parameters such as Hertzian contact stress and preload.

To test out the application of kinematic couplings to detrimental environments, two separate case studies were performed. The first case study consists of a small scale metrology device used to calibrate the home position of the ABB 6400R robot. In this application, a low-load coupling is designed for a less than ideal environment. The second case study applies kinematic coupling theory to the medium scale, high load wrist interface on the same robot. In the latter, two forms of couplings were compared, including the classic ball and groove coupling as a baseline and the three pin coupling as a new, cheap solution. Testing of prototypes of each concept shows potential for inclusion of this technology in future robot models.

Thesis Supervisor: Prof. Alexander H. Slocum
Title: Professor of Mechanical Engineering

ACKNOWLEDGMENTS

Many thanks go to Gerry Wentworth of the M.I.T. Laboratory for Manufacturing and Productivity for his assistance making the prototypes tested in the thesis. Without him, the prototypes would still be large blocks of metal sitting on my desk.

I would also like to thank Chun-Yuan Gu of ABB Corporate Research and Torgny Brogardh and Christer Lundstrom of ABB Robotics for making the project possible and providing help along the way.

Final thanks go to Alec Robertson who was our interface to the ABB Corporation. His many, many, many lengthy emails were both useful and entertaining.

TABLE OF CONTENTS

LIST OF FIGURES

LIST OF TABLES

Chapter 1

INTRODUCTION

1.1 Motivation

In the measurement and instrumentation fields, kinematic couplings (KCs) have been widely used as a method to create precise and repeatable interfaces on a variety of devices. These devices, such as optical lenses and probe mounts, require extremely high repeatability while subjected to small disturbance loads in ideal environments. Because of the strict requirements couplings place on their environments, their use in industrial settings has been relatively limited to clean areas such as semiconductor production facilities and imaging device assembly. Traditional factory environments present less ideal conditions for couplings, but equipment used in these settings could benefit greatly from improved repeatability. Although the semiconductor industry level of precision is not always necessary for general industrial machines, designers are continually increasing the stringency placed on the dimensions of their parts. In order to produce these parts, designers require better and better precision from the manufacturing equipment and machine tools. Incorporating kinematic couplings into the equipment can allow exchangeable interfaces to be more repeatable while minimally increasing the machine cost.

A prime example of this trend exists in the robotics industry. Typical industrial robots are used in the automobile industry to assemble, weld and paint cars, as well as general material handling in other industries. In these examples, small errors in the geometric properties are amplified by the robot structure and cause larger errors in the parts. The geometric

errors inherent to the robot structure are removed using calibration before the robot leaves the production facility. However, the initial calibration degrades with time due to changes in the resolver settings, thermal changes, increased loading, etc. or from discrete alterations to the robot structure. Common alterations include replacement of an individual motor or of the wrist module.

To restore the robot to optimal operation, an onsite calibration is performed. This type of calibration currently requires running the robot through a series of motions while recording the robot's Tool Center Point (TCP) with some type of measurement system. In the measurement control system, complex calculations are carried out to formulate a set of error parameters, which are used by the robot controller to correct the robot's motion. While calibration can remove most of the errors from a robot system, it requires a lengthy process of measuring a hundred or more points that can drastically reduce the productivity of a assembly line or an individual robot for up to several hours. Several hours of downtime can represent thousands to millions of dollars in lost revenue.   By incorporating KCs into the robot's structure, the requirements of the calibration procedure and measurement system can be reduced significantly. The addition of KCs to an interface improves the repeatability of the connection while often decreasing the complexity of the interface features.

1.2 Thesis Scope and Organization

This thesis will present a basic overview of the standard kinematic coupling design process, as well as a design formulation for a newer type of coupling named the three pin coupling. In addition to the design process, a shopping list of concerns for attempting KC implementation in an industrial application.

Both the design process and industrial concerns will be illustrated using two case studies of KC application on the IRB 6400 Industrial Robot available from ABB Robotics, shown in Figure 1.1. The first case study follows the development of a small scale removable device nicknamed the "Wonder Wyler" unit, which is used to calibrate the rotary resolvers

Figure 1.1 ABB IRB 6400 Robot

on each motor. To use the device, a magnetized kinematic coupling secures the unit to the robot for initial calibration before the robot leaves the production facility and for subsequent recalibrations after a major structural change such as a motor replacement. The magnitudes involved in this application include forces of around 30 N with a device size of approximately a 50 mm cube.

The second application details an effort to improve the repeatability of the wrist to upper arm interface on the IRB 6400 Robot. The wrist unit of the robot consists of two motors for the last two degrees of freedom of the robot's six degrees and the interface from robot to tool. The existing coupling constrains the interface using a pinned joint, which signifies that the repeatability of the coupling is determined solely by the tolerancing of the joint features. By incorporating kinematic coupling features into the interface, the repeatability of a wrist interface becomes a function of items such as surface finish and preload, while only the interchangeability of separate interfaces remains as a function of the tolerances. While the functioning of the external calibration device depends mostly on the environmental quality, the second application combines the effects of a detrimental environment with those of a medium-high loading situation. The magnitudes involved in this applica-

tion include forces of around 30,000 N with an interface size of approximately 200 mm by 200 mm.

Thesis Organization

The second chapter will present the basics behind coupling design, as well as the problems to be addressed in a factory setting. Chapter three moves into the small scale coupling design, with a detailed description of the design development. The fourth chapter addresses the design of the medium scale coupling. The final chapter will present some conclusions and suggestions for future work. Rather than pepper this document with references and formulas, the appendices contain a list of references grouped by the technical area and several sets of formulas presented to further explain the design process.

Chapter 2

DESIGN OF COUPLING INTERFACES

2.1 General Coupling Description

In precision machine design, one of the most important steps in designing a machine is the consideration of the effect of interfaces between components. A badly designed interface can vary from costly difficulties such as additional control or calibration to machine failure when degrees of freedom are improperly constrained. In order to avoid these problems, engineers have developed a series of deterministic tools known collectively as kinematic couplings that allow for interface features to be designed to maximize performance. The boundaries of kinematic coupling applicability has been expanded in recent years to high load, industrial areas with the introduction of high load couplings using "canoe ball" couplings developed by Slocum (Slocum, 1992b) and quasi-kinematic couplings developed by Culpepper (Culpepper, 2000). These and other coupling flavors can be combined into a design menu, which allows the designers to select the proper coupling for a specific situation. Table 2.1 summarizes the major coupling types and their relative abilities. The following sections in this chapter will give a short description of each coupling type, as well as a overall description of the design process for the kinematic coupling and three pin coupling types. The chapter will end with a description of some of the major parameters that require consideration when employing any of these coupling types in high load, industrial settings.

TABLE 2.1   Summary of Various Relative Coupling Performance Criteria

Coupling Type	Contact Type	Repeatability	Stiffness	Load Capacity	Industrially Ideal
Basic Pin Joint	Surface	Poor	High	High	Fair
Elastic Averaging	Surface	Fair	High	High	Good
Planar Kinematic	Mixed	Good	High	High	Good
Quasi-Kinematic	Line	Good	Medium to High	High	Good
Kinematic	Point	Excellent	Low	Varies	Poor

2.2 Coupling Interface Types

When designing a coupling, the precision engineer can most easily distinguish the different coupling types by investigating the types of contact that occur between the coupled interfaces. The basic types of contact are surface, line, and point contact, in order of increasing repeatability.

2.2.1 Pin Joints and Elastic Averaging

The simplest coupling design consists of surface contact, which generally occurs with direct contact between large, relatively flat interface features. Because surface contact couplings have many possible contacts spread over the interface, deterministic design becomes difficult and repeatability depends mostly on flatness, finish, and other tolerances. Generally, direct interface contact can constrain only three degrees of freedom, which requires the incorporation of additional alignment features into the design for complete constraint of the six degrees of freedom. The most common alignment geometry are pins, due to low cost and easy implementation for non-precise applications; however, strict tolerances or compliant geometries are required to achieve a reasonable repeatability. Without compliance, pin joints can easily destroy parts when the alignment features

jam or deform. Compliant geometries, such as dovetails, grooves, and rails, improve repeatability of an interface by enforcing geometric congruence through predictable elastic deflections and the removal of irregular surface features through wear-in.

In many industrial applications, preload to secure the joint is applied using bolts normal to the interface surfaces. Because of the frictional contact of the surfaces and the bolting load, surface contact couplings provide maximum stiffness and load capacity, which makes them suitable for most industrial applications where precision is not the crucial functional requirement.

2.2.2 Quasi-Kinematic Couplings

The next level of surface contact is the quasi-kinematic coupling, which consists of line contact situations such as a cylinder on a flat or a ball in a cone. By reducing a surface contact to a line, over constraint is reduced to only two degrees of freedom. Since line contacts only weakly overconstrain an interface, more deterministic relationships can be formed to provide improved repeatability. In industrial settings, line contacts do not appear as often as surface contacts, but the optics industry has made use of line contacts for aligning lenses in cylindrical capsules in v-grooves. Recent work by Culpepper (Culpepper, 2000) has developed a framework for designing and implementing quasi-kinematic couplings for high load, industrial environments, specifically in the assembly of an automobile engine.

Since quasi-kinematic couplings reduce the amount of surface interaction area, less useful area is available for the distribution of stress. Therefore, quasi-kinematic couplings can no longer support the highest loads with the best stiffness, but can provide improved precision with reasonable stiffness. Culpepper's design combines quasi-kinematic couplings using revolved line contacts with predetermined and predictable plastic and elastic deflections to optimize load capacity and stiffness, without sacrificing repeatability.

2.2.3 *Planar or Directional Kinematic Coupling*

The next coupling type, the planar or directional kinematic coupling, can be a combination of all three types of contact. For example, a planar coupling consists of a large surface contact area at the interface along with specially designed line or point contacts to constrain the free degrees of freedom. A directional coupling could be any type of coupling, which has precision alignment designed to repeatably constrain specific directions, while relying on surface features, tolerances, etc. in noncritical directions. The mixed contact coupling type has been formulated in this thesis as the three pin kinematic coupling, which uses a large surface area and three line contacts on three pins. Preload is applied by lightly torquing a bolt normal to one of the pins and more heavily torquing securing bolts normal to the interface. More details will be given for the three pin coupling later in this document.

Due to the mixed nature of these coupling, repeatability, load capacity, and stiffness are all a function of the individual design. Overall, planar kinematic couplings can provide high stiffness and load capacity with moderate repeatability.

2.2.4 *Kinematic Couplings*

The final coupling type, a fully kinematic coupling, represents the gold standard of couplings by using individual point contacts that each constrain a single degree of freedom. Because the interaction between the interface surfaces can be described by six distinct points, closed loop mathematics can be formulated to deterministically describe the relationship between the surfaces. In reality, point contacts must typically tolerate high loads, therefore the theoretical point contacts deform into Hertzian contact ellipses under large applied loads. The main limit to the repeatability of a kinematic coupling is the surface finish of the contact regions, while load capacity and stiffness are limited by the Hertzian contact stress.

By far, the most common form of the standard kinematic coupling is the ball-groove coupling, which interfaces three balls on one component to three grooves on the opposing

component. The balls and grooves are placed on the three points of a planar equilateral triangle with the triangle sides coincident to lines passing through the contact points. The typical coupling structure is shown in Figure 2.2, while the standard coupling geometry terminology is shown in Figure 2.3.
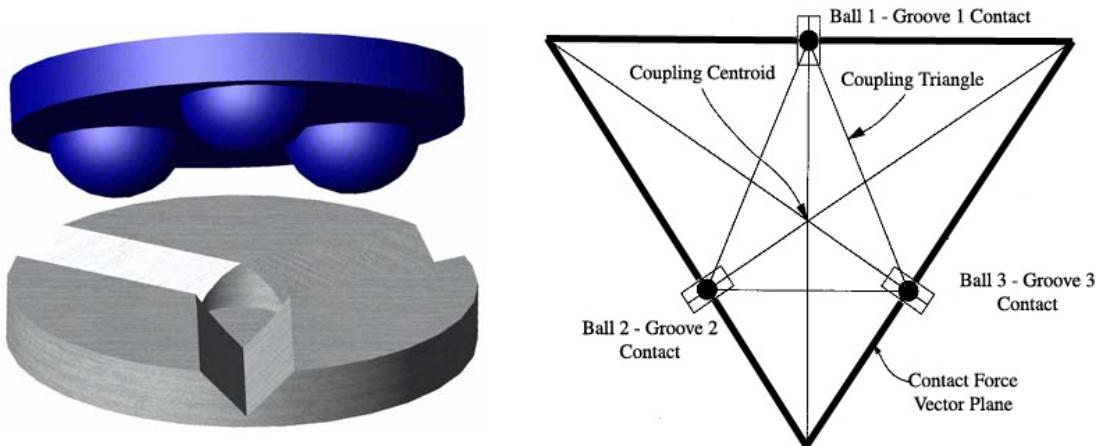
Figure 2.1   Three Ball - Three Groove Coupling   **Figure 2.2**   Standard Coupling Geometry (Slocum, 1992a)

2.3 Design of Standard Kinematic Couplings

2.3.1 General Coupling Design Process

As mentioned above, the pure kinematic coupling can provide the most precise alignment interface. Much work has been published on the general design process of standard kinematic couplings. For a more detailed description of the design process, one should refer to the work of Slocum (Slocum, 1992b). Many years of work by Slocum and his students have produced a fairly standardized mathematical procedure for designing kinematic couplings. Originally formatted in a convenient Excel spreadsheet, the mathematics necessary to design a coupling were transferred to MathCAD and are included in Appendix A, with a few improvements such as off center loading. In the appendix, the basic process for coupling design begins by establishing the geometry of the coupling and the individual components. Each component is defined by a location on the main coupling circle, as well as a

vector describing the normal of the interface surface at the theoretical contact point. In addition, the preload and disturbance forces must be specified so that the Hertzian contact stress and deformations at the ideal point contacts can be determined. Two quick checks for design success are to verify that the Hertzian stress stays less than the allowable contact stress and that the contact forces should not reverse direction. The position and force vectors are then assembled into matrices and combined with the Hertzian deformation to solve for the error motions of the coupling under the disturbance loading. Throughout the design, several other critical parameters like coupling stiffness, reaction forces at the points, and contact ellipse dimensions can be calculated.

2.3.2 Specific Design Considerations

Geometric Stability

In addition to the basic mechanics of the design, there are additional design considerations that must be addressed for a coupling to work. The first consideration, geometric stability, can be generally defined that a stable coupling is a coupling that will remain properly constrained under design loads. Stability requires specific attention for designs that stray from the ideal geometry of 120 degree spaced groove to groove angle. Figure 2.3 shows a 2D representation of different groove orientations and a relative statement of the coupling stability. One of the most useful tools to analyze stability is the well known kinematics con-
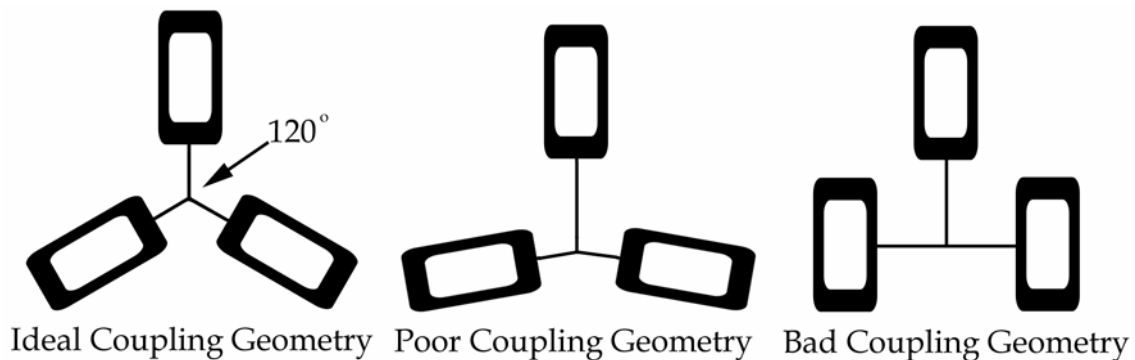
Figure 2.3 Coupling Geometry Stability

cept of instant centers, which is well described by Blanding in terms of proper constraint (Blanding, 1999). By determining the instant centers of two elements of a coupling, the third element can be located to provide maximum stiffness. The most stable coupling is one where each of the three instant centers is the same distance from the coupling centroid with the configuration as shown in the first schematic of Figure 2.3. This equal placement of constraints creates equal resistance to rotation at each instant center. If the coupling angles are changed as in the second schematic, the instant center of one element moves further from the coupling center than the other two instant centers. Increased distance between the instant center and the constraint introduces a longer moment arm about the coupling centroid for the constraint forces at the distant coupling element. The constraining moments about the other instant centers decrease, causing a non-symmetric stiffness in the coupling. If the angles keep increasing, stiffness in one direction can become negligible, causing instability to any disturbance force in that direction.
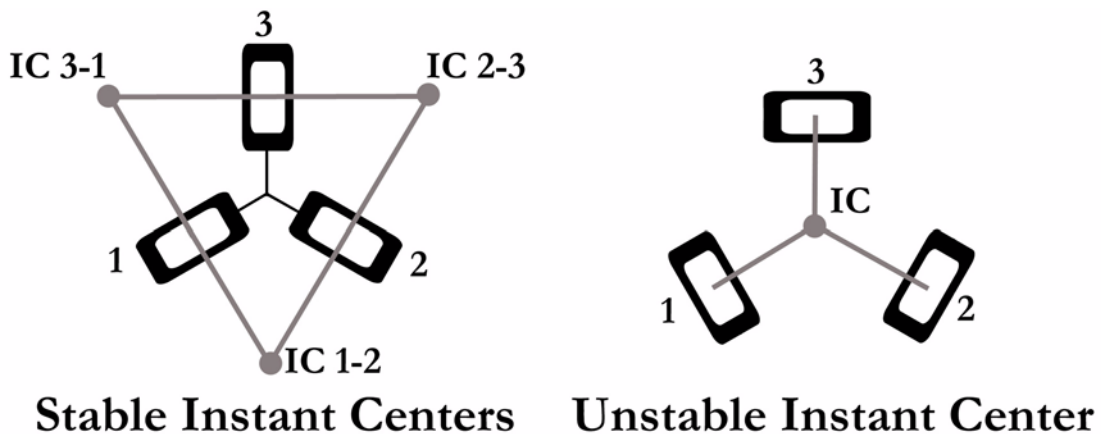
Figure 2.4   Instant Centers and Stability

In Figure 2.4, two sample instant center schematics are shown. The first schematic indicates the 120° configuration above where the instant centers are located at a distance from each other to create maximize stability. The second schematic shows a configuration that could easily be mistaken to have stability as all six points are in contact in 120° form. However, an analysis of the instant centers shows that all three instant centers coincide at

the center of the coupling triangle. Any disturbance force applied to this coupling will cause rotation about the instant center with very little resistance, as no constraint forces can be applied normal to the moment arm created from the constraint to instant center. For a design similar to the third schematic in Figure 2.3, the instant centers can occur at infinity, which allows for translation in the direction normal to the lines connecting the constraint and instant center. These two designs are inherently unstable, unless sufficient friction can be introduced at the interface to resist motion along the groove. While these couplings may represent bad designs for exact constraint of interfaces, differential stiffness and frictional constraints can be cautiously included in designs where these features may be desirable.

In addition to static stability, dynamic stability must also be considered in designs were high loads are applied in directions that change over time. In the first diagram, maximum dynamic stability occurs when the planes containing the contact force vectors intersect to form a equilateral triangle using similar logic as above. This configuration provides maximum resistance to a disturbance in any direction by properly providing a supporting surface. It can be easily seen in the second and third diagrams how a disturbance can easily cause motion in the coupling. When the design introduces dynamic loading or moving geometry, the coupling must also be checked for dynamic stability. Dynamic instability can be initiated when the forces at the interface contact points suddenly reverse or when the contact force vectors become aligned with the direction of the grooves. To prevent these dynamic instabilities, additional preload can be applied (within the allowable contact stress) and physical stops can be used to prevent improper motion.

Interface Stiffness

Integrally related to the stability of the coupling, stiffness can become a major influence on the applicability of a standard kinematic coupling to an industrial design. When the coupling components are arranged in the 120 degree configuration and the groove faces are perpendicular, the coupling provides equal stiffness in all directions. Change in the geometric parameters of any of the components will introduce changes in stiffness that

must be considered if they are in sensitive directions. Since these couplings rely on six point contacts to support interface loads, stress and deformation levels can rapidly increase, causing a very undesirable change in stiffness properties when compared to a bolted joint. Changes in stiffness when using three ball - three groove couplings can amount to an order of magnitude or more reduction in stiffness. Careful comparison of finite element simulations of the original joint with approximations of the ball - groove interface are instructive for order of magnitude comparisons of the stiffness change. Since Hertzian effects at point contacts are not currently well modeled in commercially available FEA products, several approximations can be used to model the interface contact. The most accurate approximation relies on creating flexural geometries that simulate the joint stiffness predicted by traditional contact mechanics. However, careful attention must be paid to this approximation to ensure that all deflections and forces are compared at the proper locations. A less accurate method to simulate the contact is to replace the coupling geometry with a block enclosing the coupling elements. To simulate the change in stiffness of the joint, the material properties of the new block should be altered from the basic material of the structure to reflect the reduced stiffness of the coupling determined by contact theory. Appendix C contains the mathematics and further explanation of carrying out these approximations using the interface discussed in Chapter 4.

Contact Stress

Another item to be considered is the contact stress present at the interface. Due to the nature of the point contact, high Hertzian contact stresses can be present in the coupling under the preload alone. Stress analysis should be performed both concerning the static preload alone and with the maximum predicted disturbance force. In addition to the good practice of designing with an appropriate factor of safety, a ball-groove interface should be designed so that space of at least one diameter of the contact patch is left between the border of the Hertzian contact patch and the edge of the supporting components.

To counter the low load limitation present in traditional ball-groove couplings, Slocum has developed the specialized "canoe ball" element as described in U.S. patent number

5,711,647 (although not claimed). The canoe ball replaces the traditional hemispherical contacting element with a trapezoidal block with sections of a spherical surface ground onto the contacting surfaces. By grinding spheres with diameters as large as a meter onto the sides of the canoe ball, contact stress at the interface can be reduced while preserving the contacting components small size. The larger diameter creates an approximately kinematic elliptical contact patch that drastically increases the load capacity of a coupling while maintaining high repeatability. In Figure 2.5, the canoe ball is shown along with its
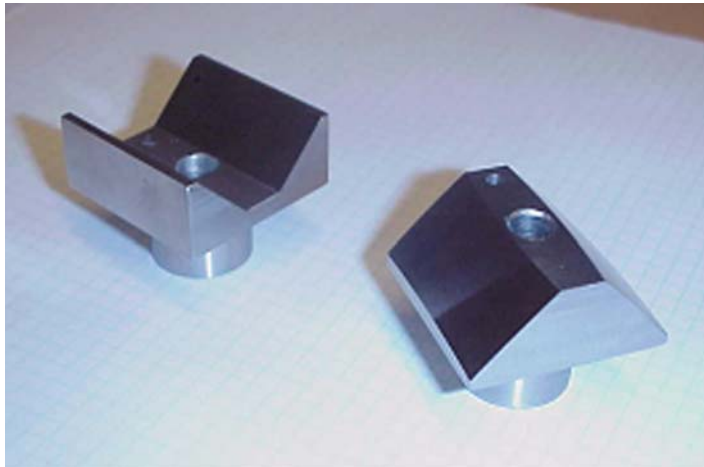
Figure 2.5   Canoe Ball and Groove Element

matching groove. Benchtop level experiments have shown repeatability of approximately one micron for the design setup in Chapter 4 and 0.1 microns in previous work by Mullenheld. For a good presentation of contact mechanics theory, Johnson provides detailed derivations (Johnson, 1985).

Surface Material Properties

Of the many factors which affect the repeatability of a coupling, the choice of material for the ball and grooves has several critical influences. As in any precision design, one of the most important factors to consider is the friction between the contacting surfaces. Friction

alters repeatability the most during initial assembly of the coupling. After each of the coupling elements touch, friction between the surfaces builds up and creates forces that impede the motion of the entire coupling from settling into its lowest energy state. Each subsequent replacement of the coupling will settle into a different position based on a complex relationship between the initial position of each contact point and the exact direction of applied force. Several techniques can be used to minimize the effect of friction, including low coefficient of friction materials such as Titanium Nitride combined with Tungsten Disulfide and proper dithering of friction. During installation, frictional effects can be easily dithered using a stepped bolting procedure and by simply tapping the interface region with a hammer. Dynamic couplings also require special attention to frictional effects to improve repeatability and response to motion.

Another important material influence on the repeatability stems from the relative hardnesses of the ball to the groove. Ideally, the best repeatability can be obtained by the combination of a hardened steel ball and groove. However, some designs may stipulate that one half of the coupling be disposable, while the opposing half must remain fixed to the rest of the structure. In these instances, it may be more useful to use hardened steel ball elements on the fixed structure and mild steel groove elements on the disposable components. This technique will help to prevent any assembly damage from being imparted on the fixed, more expensive structure and transfer the deformations to the grooves on the disposable structure. In addition, grooves can be easily milled into mild steel components using standard end mills rotated 45 degrees, while the hardened ball elements can be expensively machined or press fit into the fixed structure. When the ultimate level of precision is required, ceramics such as Silicon Nitride can be used for extreme hardness, as well as improved repeatability through decreased friction and wear-in time. During the initial assembly cycles of a single matched coupling, wear-in has been observed when coupling repeatability decreases slightly to a steady state value after many replacement cycles. This effect can occur due to the removal of surface finish aberrations by the loading and high contact stress at the point contact, as well as other interface interactions.

The final material effects involve three variations on surface geometry: surface finish, debris, and fretting. Out of the three variations, surface finish is the easiest parameter to affect during design, as the finish can be specified and measured during manufacturing. Furthermore, surfaces will tend to burnish or polish each other with increased time and load. Debris and fretting are more difficult parameters to analyze and remove, as these effects tend to develop over the lifetime of the components. In most cases, repeatability variation due to debris can be reduced by simply establishing a regular cleaning procedure to remove the debris using necessary solvents and by placing a small layer of grease on the elements. The final surface effect results from a process known as *fretting corrosion*. Fretting occurs between two surfaces of similar materials, particularly steels, when they are pressed together under large forces. On a small scale, these large forces cause surface asperities to crush together and atomically bond. When the surfaces are separated, the new bonds are ripped apart, causing the small pieces of the bonded materials to become debris on the surface. In addition, the process of ripping apart the material exposes new material to the environment. The newly exposed material can oxidize, causing a change in surface hardness as well as surface finish. Variation due to fretting cannot be easily avoided under high loads if non-stainless steels are used, so it is recommended that stainless materials, ceramics, or combinations of dissimilar materials be used. Ceramic and stainless materials also have the added benefit of being noncorrosive in many unpleasant industrial environments.

2.4 Three Pin Coupling

2.4.1 General Coupling Description

The *three pin coupling* developed for this work is categorized as a planar kinematic coupling, as contact occurs at three line or point constraints and a large surface contact. The name of this coupling is derived from the geometry of the interface, which consists of a plane contact constraining three degrees of freedom and three pins constraining motion in the plane. Each pin constrains motion by mating with a precision control surface normal to

the interface plane. To prevent pins from jamming during assembly and to remove any free motion, preload is applied to an anvil pin using compliance or some adjustable mechanism. The proper design of the pin geometry and preload force will compel the coupling to deterministically seat in a repeatable position. The control surfaces and the pins are the only elements of the interface that require accurate tolerancing, as repeatability and exchangeability is affected by the location of each element. In Figure 2.6, the basic geometry and nomenclature for the three pin coupling is shown, while Figure 2.7 shows an example of one possible coupling structure. Since each pin interfaces with a flat or curvic surface, Hertzian contact theory can be used to describe the interface stress and deformation between the cylindrical pin or ground point contact and the control surface. A standardized spreadsheet or procedure similar to that available for standard kinematic couplings is not provided for the three pin coupling, as geometry can vary sufficiently to prevent a simple closed formulation. An example of the mathematics used to describe the three pin coupling used for the small scale case study are included in Appendix B, however these calculations are only useful for this particular design case. Johnson's contact mechanics book present a thorough coverage of any contact theory that may be necessary to further describe these interfaces.

2.4.2 General Coupling Design Process

The basic coupling design process is a rather simple process, as it involves fairly standard summations of forces with regard to preloads, disturbances, and friction. In order to implement a three pin coupling, the following steps are required:

1. Specify initial interface geometry, including locations for the support pins, anvil pin, control surfaces, and preload bolts. Determine method for applying preload and estimate static and disturbance loads. To reduce complexity of calculations, transfer external forces and moments to the location depicted as the geometry center in Figure 2.6.

2. Construct a free body diagram based on initial geometry and the static load. Perform summation of forces and moments on this geometry to sustain static
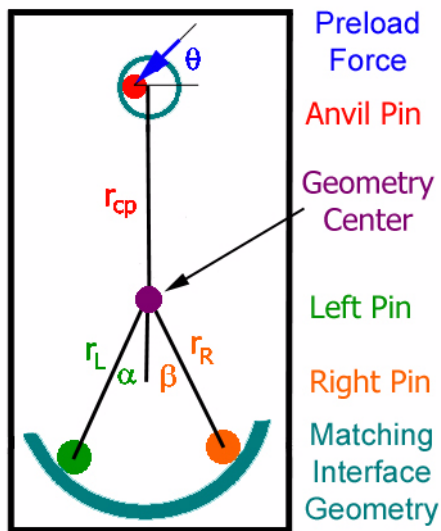
Figure 2.6   Nomenclature for Three Pin Coupling   **Figure 2.7**   Basic Three Pin Structure
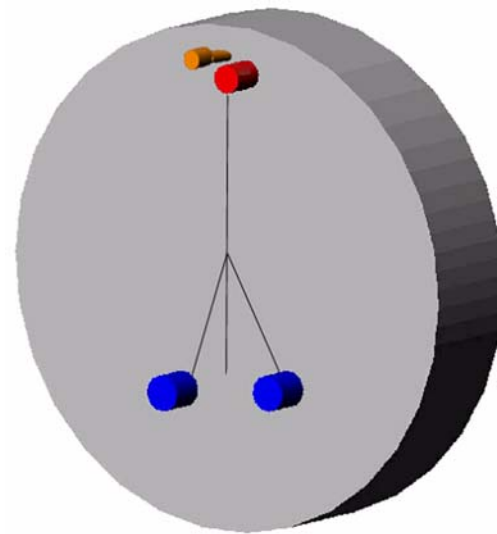
loading case. Solve for the minimum required in-plane preload necessary to ensure contact of the three pins with the control surfaces and for the minimum bolting force necessary to keep the planar surfaces in contact. Throughout the calculations, it is important to include friction from static loading (but not the bolting force) to ensure that the in-plane preload is sufficient to overcome the friction and seat the coupling with all possible initial positions of the coupling.

3. Construct another free body diagram based on the initial geometry and the disturbance loads. Perform summation of forces and moments on the geometry to sustain the dynamic loading case. Solve for the minimum required normal preload necessary to ensure contact of the three pins with the control surfaces and for the minimum bolting force necessary to keep the planar surfaces in contact. Throughout these calculations, it is important to include the effect of in-plane friction as a function of the normal loading, as the in-plane friction will help to resist moments and torques in the coupling plane. There-

fore, the bolting force must be increased to increase frictional resistance to any dynamic disturbances.

4. Using contact forces at pins, check Hertz contact stresses, bending stresses, and any other failure modes of concern. Diameters and heights of the pins and the control surfaces can be determined based on these failure possibilities. Appropriate factors of safety should be applied to the in-plane preload, bolt forces, and stresses to ensure that the design will safely seat if estimated disturbance forces are exceeded.

2.4.3 Specific Design Considerations

Preload on Third Pin

Preload on the third pin can be applied in numerous ways, depending on the geometry and restrictions of the coupled components. In U.S. patent number 5,915,678, Slocum used a form of the three pin coupling called the kinematic sheet to align printed circuit boards for the electronics industry. Three pins were placed on a surface tilted with respect to vertical, while matching notches are placed in the kinematic sheet. Preload is applied to all three pins passively by using gravity to pull the sheet into place on the positioning plane. An illustration of this preload method excerpted from the patent is shown in Figure 2.8.

In Figure 2.9, another preload method is shown using a combination of a thick, rigid anvil pin and a relatively thin and compliant spring pin. The spring pin preload method ideally operates by simultaneously inserting the anvil and spring pin into the matching hole on the opposing component. By designing the matching hole to be smaller than the maximum distance between the outer surfaces of the pins, the pins will be compressed together. Since the spring pin is more compliant than the anvil pin, the compression force will cause the spring pin to bend following standard beam theory. Ideally, the anvil pin should not deflect at all and remain in kinematic contact with the matching control surface. Preload force for this design can be specified by determining the spring pin deflection from the basic geometric parameters of matching hole diameter, spring pin head diameter, spring
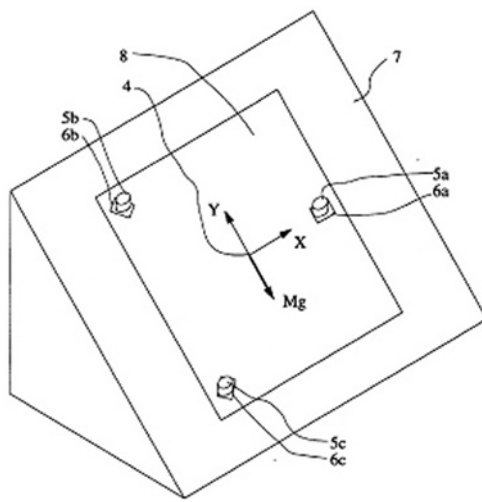
Figure 2.8 Kinematic Sheet Drawing   **Figure 2.9** Spring Pin Schematic
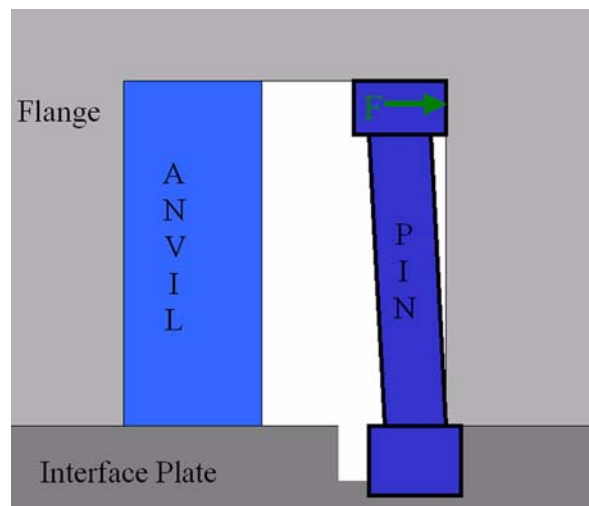
pin main diameter, and distance between the spring pin base and anvil base. This spring pin deflection can be passed through standard beam equations to determine the force created from the pin insertion. A design example for this preload method will be shown in Chapter 3.

The final preload method considered employs a simple preload bolt, aligned so that its force is applied in the necessary direction for coupling constraint. This preload method is the simplest to implement, as it requires only a threaded hole in the proper direction. However, careful attention should be paid to the free body diagram and force directions to ensure that the coupling will seat in only one location. To ensure that overconstraint does not occur, a specialized bolt can be used with a copper tip to allow for some compliance at the contact point.   Also, a simple wooden prototype can save much time verifying that the direction of the preload will properly seat the coupling.

Preload in Bolts

Preload applied using the bolts normal to the interface are very important to the successfulness of the three pin coupling under dynamic situations. To simplify calculations and improve precision, preload bolts should be located so that they pass through the centers of

the pins. Often, the design will require that bolts be placed at separate locations or that more than three bolts will be needed to supply sufficient force. In this situations, the design must address bolt arrangement to prevent asymmetric bending of the interface plane. Bickford and Nassar have compiled a very useful handbook that can be helpful in properly designing the bolting configuration (Bickford, 1998).

Friction on Interface

Friction on the large contact surface provides the three pin coupling with additional ability to sustain large forces and moments in the plane of the coupling. To create interface friction, large normal forces must be applied to the surface using bolts. If the required bolting force exceeds the capability of the desired or possible bolting pattern, the friction coefficient of the interface surfaces must be increased by changing the interface material using coatings, by changing the quality of surface finish, or by including a dimpled friction plate between the interface surfaces. Any changes in frictional properties must be reviewed in the second step of the generalized design process to ensure that the in-plane preload is sufficient to seat the coupling.

2.5 Factory Issues

In addition to general design concerns for creating interface couplings, some helpful guidelines exist for the design of the assembly procedure. Often, these techniques can change the repeatability by an order of magnitude or more, but can be easily overlooked by installation and maintenance staff in a factory environment.

2.5.1 Lubrication of Interface

As mentioned earlier, the presence or lack of friction on interface surfaces can change functionality of a coupling. In the case of the ball and groove kinematic coupling, friction at the interface is an undesirable property, as it will tend to prevent the coupling from settling into the lowest possible energy state. The addition of lubrication to the surfaces after cleaning the surface can improve repeatability by a significant factor as less energy can be

stored by the friction. Lubrication can be added using a swab of simple high pressure grease. However, spray lubricants are more desirable as the chance of contaminants being introduced to the interface is less in the spray lubricants than solid grease.

In the case of the three pin coupling, it is desirable that two separate frictional states occur: low friction on the edges of the pins and the control surfaces and higher friction at the interface plane. Similar reasons for low friction in the kinematic coupling exist for the in-plane elements, as friction will determine the initial location of each pin to control surface mating. Higher friction is desirable at this interface as friction at the interface increases the coupling's dynamic load capacity. Techniques such as dimpled friction plates and changing surface properties can be used to improve frictional properties. In situations where friction is a major cause of non-repeatability, dithering of friction can be employed by tapping the interface region with a hammer.

2.5.2 Installation of Bolts

In many non-precision applications, it may be sufficient, but not wise, to tighten bolts by hand and then give the torque bar a "good kick or pull" to tighten it as is often done in industrial settings. However, careful attention must be paid to the method used to install and torque the bolts when coupling precision components. Each time the components are coupled, new bolts should be used to prevent inaccurate preload caused by bolt stretch. In addition, both internal and external threads should be cleaned and lubricated before each use. Small contaminants or high friction present in the threads can cause jamming of the bolts or redirect the preload into breaking friction, rather than exerting a clamping force. When installing the bolts, the following sequencing should be used to optimally introduce the load:

1. Clean and lubricate all threads.

2. Insert all bolts into the components and lightly finger tighten without applying any torque.

3. Torque each bolt to 10% of the final load to initialize contact at each interface. If multiple bolts are used, they should be torqued in a pattern where the following bolt is on the opposite side of the coupling. This pattern prevents the creation of an asymmetric bending moment across the interface caused by the tightening of several bolts on one side of the coupling. Each subsequent coupling should follow the same bolting pattern to ensure repeatability between couplings.

4. Torque each bolt to 50% of the final load to counter the initial static friction. Torque pattern should be consistent with previous pattern.

5. Torque each bolt to 100% of the final load to apply final clamping load. Torque pattern should be consistent with previous pattern.

2.5.3 Cleanliness

Cleanliness is always important in precision machines. In any type of couplings, contamination is important within the precision contact elements as it can change the location of the contact region, both through direct interference with the contact and through damage imparted on the surfaces. If damage occurs on the disposable component, minimal cost is incurred by replacing the component, while damage on the fixed structure can require replacement of a large part of the structure. Cleaning procedures as simple as a blast of compressed air to more complex freon cleanings can preserve parts and maintain repeatability for a low cost. However, cleaning procedures may remove the necessary layer of lubrication, allowing corrosion, fretting, or friction to disturb the design so lubrication must be repeated.

Chapter 3

SMALL SCALE DESIGN CASE STUDY: THE CALIBRATION CUBE

3.1 Background and Problem Description

3.1.1 Background (Robertson, 2001)

In the field of industrial robotics, many different calibration methods exist to help reduce error in the robot system. One of the most common calibration methods, locating the manipulator home position, requires that the robot be positioned with all joint angles specified to have a value of either zero or 90 degrees. For large industrial robots, this home position must be repeatable to within 0.2 mm in Cartesian space at the end point of the robot. Using robot kinematics, the Cartesian requirement can be transformed into a required joint angle repeatability of 0.01 degrees.

During a standard production run of ABB industrial robots, each robot undergoes several calibration procedures, including a complex procedure for finding the home position. Once the home position is found, specialized error parameters are formulated based on the robot kinematics and stored in the controller. These parameters are valid for the initial robot configuration, however, they may change over the lifetime of the manipulator, especially if components are exchanged. If the calibration process used during manufacturing could be improved and simplified, the robot could be recalibrated whenever necessary, without requiring the expensive and complicated measurement systems.

To improve the calibration of the home position, ABB engineers first wanted to simplify the method of calibration. The home position can be found using one of the following three separate methods of calibration:

1. Relative calibration - Expensive process that requires each component in the robotic structure to be defined relative to the previous component. Accuracy from relative calibrations can vary based on the accuracy of the robot components.

2. Optimal calibration - This process uses a measurement system combined with kinematic models of the robot to measure many positions of the robot and correct any errors present in structure. Accuracy from optimal calibrations can vary based on the robot positions and kinematic model.

3. Leveling based calibration - Process uses simple electronic levels known as inclinometers to easily orient each component of the robot structure with respect to the angle read by the inclinometer.

Because leveling methods are much simpler and cost effective, leveling based calibration was chosen for the new device. However, several aspects of the design must be reconsidered to reasonably achieve the required repeatability. The overall precision of the new device combines the accuracy of the robot control system with the repeatability of the device structure and the interface between robot and device. A baseline home position repeatability can be estimated from the critical component of the robot control system, the resolver accuracy, which is typically on the order of 100 micrometers based on ISO standards for a defined speed and payload.

In order to test out the concept of a leveling system, ABB engineers developed a prototype unit using inclinometer sensors from the Wyler AG Zerotronic System. These sensors employ a digital capacitance system that measures the deflection of a small pendulum mounted between two electrodes. Originally, two sensors were mounted on separate right angle plates that were placed at several mounting points on the robot. One sensor was

placed on the base of the robot to provide a reference angle for each of the subsequent measurements. To measure each joint, the second leveling sensor was placed at one of four locations on the robot. Each joint of the robot is then manually moved to a position that corresponds to the predefined angle. Testing of this initial system presented mean recalibration error of 1.0 mm measured at the tool interface of the robot. This error can be broken down to show that half of the error is a result of the mounting interface, a third is a result of the plate construction, and the remaining error is considered random.

To improve the initial device, the prototype was reduced to a single right angle plate with the two sensors mounted perpendicular to each other within the structure. Operation of the calibration procedure was also improved with automated software to adjust the position of the robot joints to match the values required by the sensor values. Figure 3.1 shows the
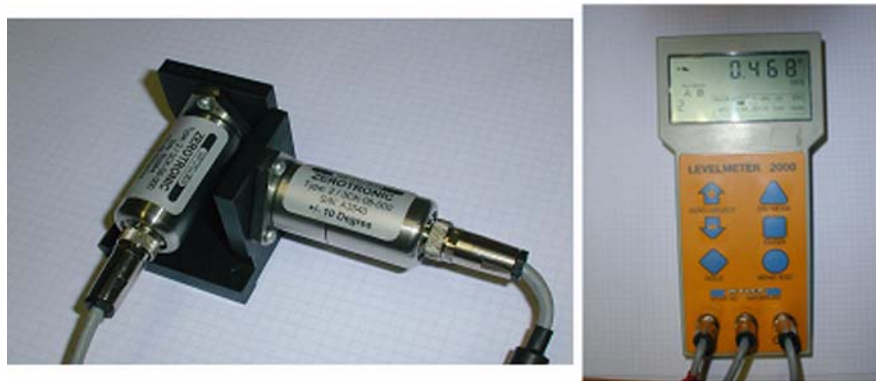
Figure 3.1   Wyler Sensors and Accompanying Meter

resulting sensor unit along with the meter. With the new device, the unit was placed on the base to measure the reference values. The same unit is moved to four additional points on the robot, as shown in Figure 3.2, to measure the remaining joints.

3.1.2 Problem Description and Function Requirements

At this point in the design process, the main component of the error budget to be addressed was the coupling interface between the sensor unit and the robot. Slocum and Willoughby
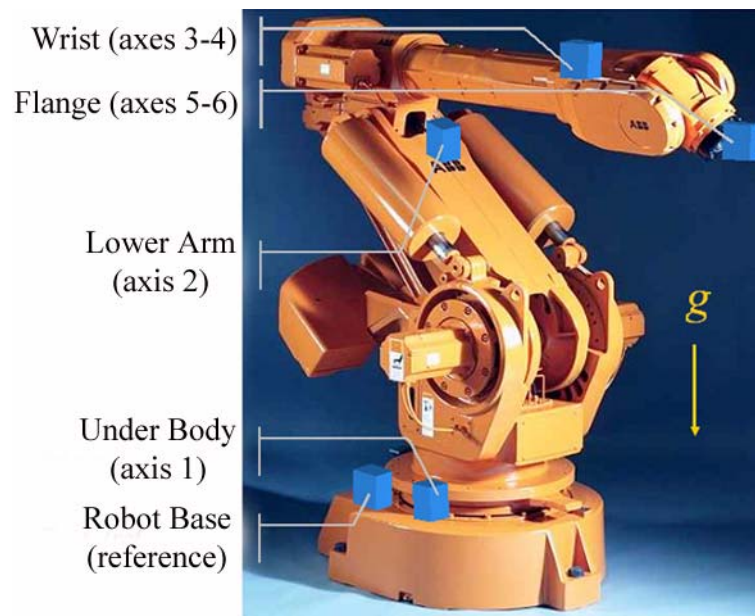
Figure 3.2   Location Point for Levelling Device on Robot

become involved in the design of the device, known as the "Wonder Wyler", to assist with improvement of the coupling process. After some discussion, a set of initial functional requirements were developed:

1. Reduce error in coupling of device to robot to allow for 0.05 degree accuracy at each joint.

2. Unit should be compatible with several models of robots without requiring extensive change to the robot structure.

3. No changes can be made to the interface on the tool flange, which has space limited to 50 mm by 50 mm on the smallest robot. ABB engineers require that an extra interface plate be placed between the sensor unit and the robot if the unit cannot attach directly to the flange.

4. Coupling should be easily removable using simple preload application, but will not fall off. Mechanical connections are desired for extra security.

5. Coupling should prevent improper installation.

During the course of the project, these requirements were changed frequently as ABB's customer needs were fine tuned. The final list of requirements were as follows:

1. Reduce error in coupling of device to robot to allow for 0.05 degree accuracy at each joint.

2. Coupling should be easily removable using simple preload application, but will not fall off.

3. Unit should be compatible with several models of robots without requiring extensive change to the robot structure.

4. Coupling should prevent improper installation.

3.2 Design Development

As the design progressed, the functional requirements coalesced into four major design tasks: coupling type, securing force, coupling location, and dynamic coupling. Each of the four tasks encompasses many design decisions for all of the functional requirements due to their highly coupled nature.

3.2.1 Coupling Type

Standard Ball and Groove Kinematic Coupling

The choice of coupling type for the interface is the most crucial design decision to affect the precision of the device. To design the coupling, the requirements of the coupling type were low load capacity, high repeatability, and medium cost. Since the device was small, standard ball and groove kinematic couplings could be used with out inducing high contact stresses. Physical construction of the coupling would consist of three balls aligned in the traditional triangular pattern placed onto a side plate of the unit with matching grooves placed on the desired measurement locations.

On the device side of the coupling, the inclinometer unit consists of three plates accurately mounted in an open cube structure, with three spheres placed on the outer surface of the

bottom and front plates. Rather than machine balls into the surfaces, standard tooling balls were press fit into precisely located holes. The cost of the coupling could be significantly lowered by using the press fit balls, since tooling balls can be purchased fairly cheaply from a wide number of vendors with extremely good tolerances. In order to secure the unit, a minimum preload of 15 newtons was required to hold the approximately 1 kg unit in place. A factor of safety of 2 was applied to the design to ensure that the device would not fall off during any movements of the robot. Although the maximum forces on the interface are quite low, the standard kinematic coupling design was performed to verify that contact stresses were sufficiently low while the preload is successful at preventing the reversal of any contact forces. To prevent improper device installation, the angles between the grooves could be changed from the standard 120-120-120 degree setup by 5 degrees without significantly affecting the coupling stability. Figure 3.3 shows a CAD model of the design using half inch balls mounted in a 20 mm circle on a 50 mm by 50 mm plate of steel and Figure 3.4 shows the CAD concept of the sensor unit comprised of an open cube structure.
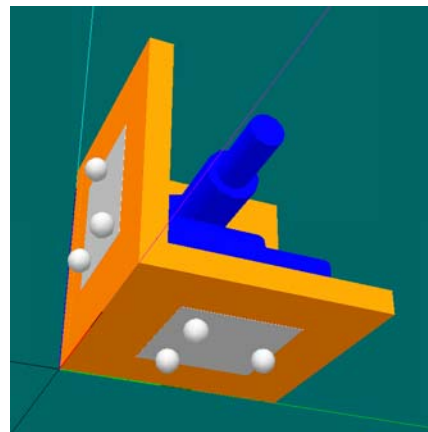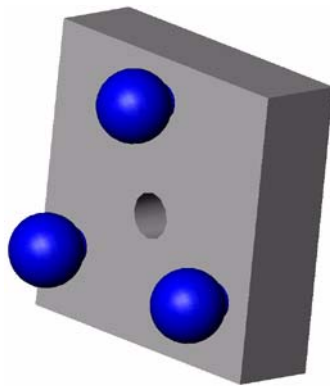
Figure 3.3   CAD Model of Side Plate   **Figure 3.4**   CAD Model of Open Cube Structure

On the robot side of the coupling, it was necessary to create three grooves on five locations, represented by the blue squares shown in Figure 3.2 above. Initially, grooves were machined into separate plates that were bolted into existing bolt holes on the robot struc-

ture. After some preliminary testing, it was discovered that bolting additional groove plates on the robot did not have sufficient repeatability due to the inaccuracy of the bolting procedure. A simple cost versus accuracy analysis was performed showing that the cost of accurately mounting groove plates to the robot each time the device was used exceeded the cost of accurately machining or casting grooves into the robot structure. V-grooves with an angle of 90 degrees are used to optimize stability and for ease of manufacturing.

Flange Mounting and Three Pin Coupling

Before the ABB engineers had relaxed the requirement for placing grooves into the robot structure, several different design variations were developed to allow the "Wonder Wyler" unit to attach to the flange without requiring changes to its critical features. The tool flange, located at Flange (axes 5-6) in Figure 3.2 and shown close up in Figure 3.5, is the high load connection interface between tools and the robot. The design variations included
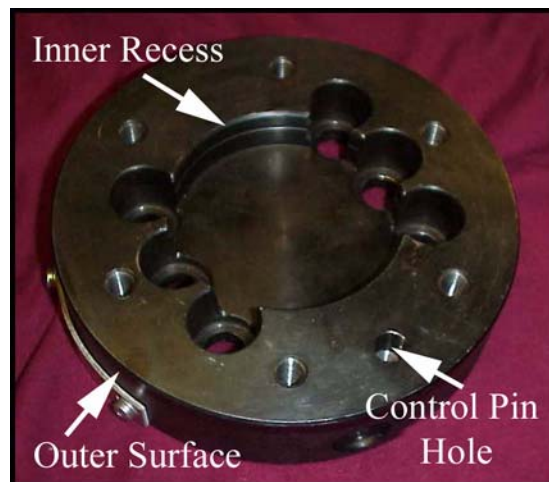
Figure 3.5   Flange Interface on ABB IRB6400 Robot

a three pin coupling that interfaces with the toleranced features on the flange and several concepts for including coupling features on non-critical surfaces of the flange. In this sec-

tion, only the three pin design will be discussed, while the latter designs will be presented in a following section.

After the initial project discussion with the ABB engineers, it was determined that a three pin coupling could work as an interface to an extra plate between the flange and the "Wonder Wyler" unit. Pins on one side of the plate would easily couple with the toleranced features on the flange (noted on Figure 3.5), while grooves on the reverse side would couple with the sensor unit. The initial design concept consisted of two pins resting against the inner recess of the flange, a pin that would rest inside the control pin hole, and a spring plunger that would provide a locking preload force. To model the interaction of the pins with the flange, a detailed mathematical model was developed to describe the forces acting in the system and is included in Appendix B. Concurrently, several basic wooden prototypes were constructed to visually assist the design of three pin coupling. Figure 3.6 shows the various components of the wooden model uncoupled, while Figure 3.7 shows the coupled model with the spring plunger direction indicated by the black arrow. In

Figure 3.6   Components of Three Pin Model
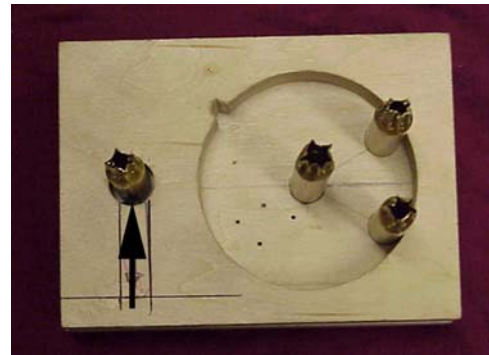
Figure 3.7   Assembled Three Pin Model

Figure 3.6, the left component represents the critical features of the flange, including the control pin hole and inner recess, as well as a side hole for insertion of the spring plunger. A spring plunger consists of a small, spring loaded pin with a round head placed inside a threaded casing, as shown in the center of the figure. For the three pin coupling, the spring

plunger is used as an adjustable preload. The right component represents the three pin plate, with a fourth center pin used for additional adjustments.

As the design progressed, it became apparent that the spring plunger design would be unsatisfactory as the flange would require major modification to accept the plunger and the plunger would occupy too much space for the smaller robot designs. To reduce the size of the design, the spring plunger was removed from the design and replaced by an additional feature on the interface plate called the spring pin. This pin would also reside inside the control pin hole on the flange and would provide the preload force by resistance to the bending of the pin. In Figure 3.8, a possible design for the interface plate is shown using an asymmetric split pin, highlighted in the box. To create the preload force, the split pin is sized slightly smaller than the matching hole. The repeatability of the contact is ensured by placing the gap off center, which allows the larger section to remain rigid compared to the smaller section. The smaller section is sized to customize the preload. Due to the complicated machining requirements of this design, a simpler design was formulated as shown in Figure 3.9, using a straight dowel pin as the spring pin. The spring pin action is similar to a cotter pin, where two pins separated by a small gap are forced into a slightly smaller hole. As in the split pin design, one of the two pins has a diameter significantly smaller
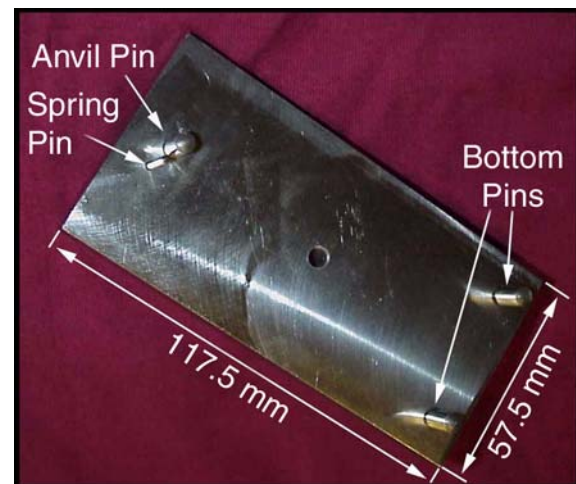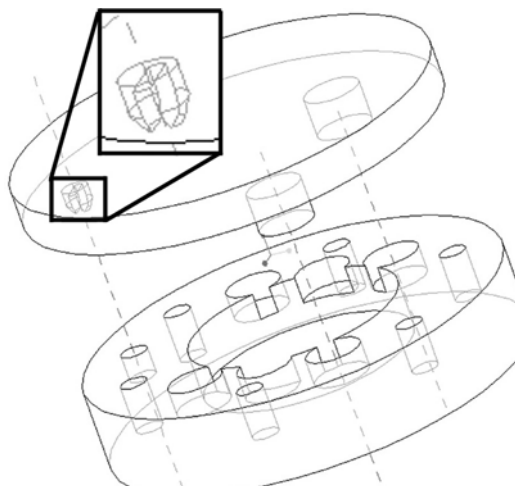
Figure 3.8 Asymmetric Split Pin Design   **Figure 3.9** Prototype of Three Pin Coupling with Spring Pin

than the rigid contacting pin, called the anvil pin. Using beam theory, the pin deflection caused by the diameter reduction can be translated into the preload force with relatively simple calculations. These simple calculations are included in Appendix B. The prototype shown in Figure 3.9 is capable of producing a 20 Newton preload force when a deflection of 0.5 mm is enforced on the spring pin using the flange geometry. In Figure 3.10, the
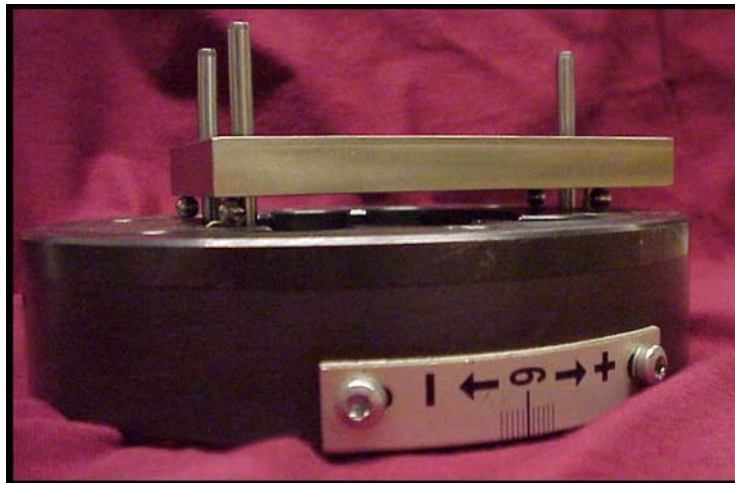
Figure 3.10   Three Pin Prototype Coupled with Flange

three pin coupling prototype is shown successfully coupled with the ABB IRB6400 robot flange. The small space between the interface plate and flange would normally be undesirable for a finished product as the design cannot be deterministically located along the flange plane. When designing the prototype, this space was included to allow future testing of three dimensional stiffness of the coupling with minimal interface friction. To reduce friction yet preserve some constraint, 6 mm diameter balls were placed between the plate and flange to allow the plate to move in the plane of the flange, but still be constrained for out of plane motion. A tolerance analysis was performed using a flexible CAD model in SolidWorks to show that repeatability of 0.05° is possible with tolerances of ±0.05 mm.

After the ABB engineers had relaxed the requirement that no changes be made to the structure of the flange, it was quickly determined that the best design would be to include grooves integral to the flange structure. The same groove pattern used on the other mounting locations were machined into a cylindrical insert that could be press fit into an existing flange as an initial test. Figure 3.11 illustrates the grooved insert plate in dark red, as well as demonstrating how the sensor unit fits into the available space.
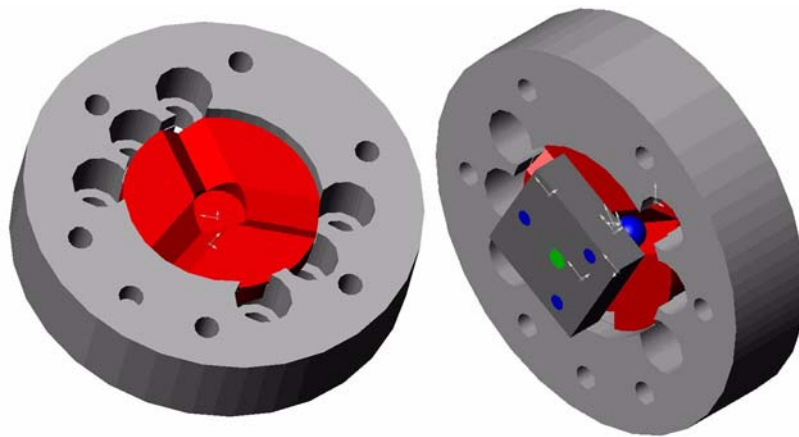
Figure 3.11   Insert Plate in Flange, Sensor Unit on Insert Plate

3.2.2 Preload and Securing Force

The next crucial design element to determine is the method of preloading and securing the "Wonder Wyler" sensor unit onto the corresponding grooves. As mentioned above, the required preload with safety factor is 30 Newtons. Due to the small size of the components, all force application tools would ideally be located in the center of the coupling. Centralizing the force also assists with an even balancing of preload at each ball to groove contact. Three types of securing mechanisms were considered for the sensor unit: physical attachment using a bolt, physical attachment using a "coat hook" style connector, and magnetic attachment. In addition, some quick operating push button fasteners were considered for use, but were discarded immediately due to cost and implementation issues.

Attachment using a Bolt

The simplest and most obvious physical method of securing the sensor unit consists of a single standard bolt that passes through a clearance hole on the unit and threads into a hole at each mounting location. However, several problems became apparent when trying to incorporate bolts within the physical constraints of the sensor unit. As shown in Figure 3.4, one of the inclinometer sensors must be mounted at the center of one coupling triangle, while both sensors make access to the bolt difficult for the other coupling plate. While it is conceivable that the sensors could be rearranged to allow for the bolts to be used, traditional design for assembly rules strongly recommend that obstructed assembly procedures similar to this concept should be avoided. ABB engineers also preferred that some form of quick lock and release ability be available, rather than the lengthy process required to properly preload bolts.

Attachment using "Coat Hook"

During the early stages of design, the second securing concept was formed by ABB engineer Alec Robertson due to the desire to maintain a physical securing connection between the sensor unit and robot at all times. This concept was termed the "coat hook" solution due to the similarity of the attachment element to coat hooks commonly found on airplanes and trains.   The construction of this device consisted of a threaded knob that is
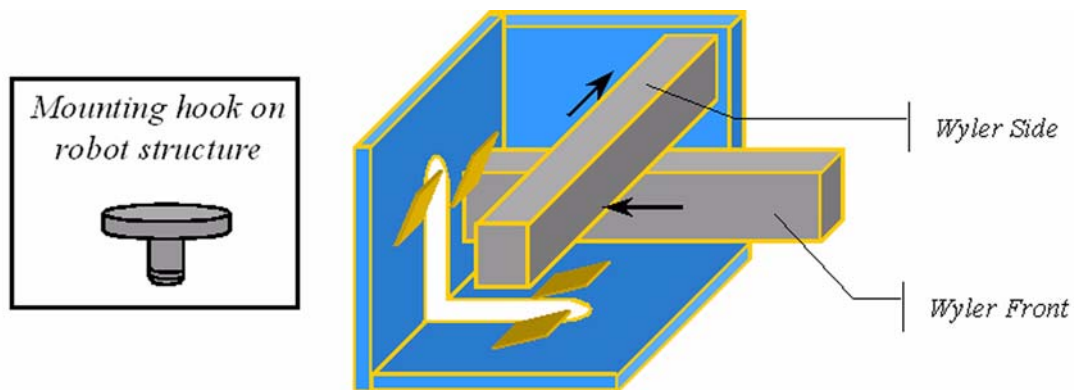
Figure 3.12   Schematic of Coat Hook Design

secured at the center of each groove set on the robot. On the sensor unit, special notches and slots are cut to receive the mounting hook. Springs are incorporated either into the hook or the sensor unit to apply preload force, as shown by the small angled yellow planes in Figure 3.12. Assembly of the device occurs by carefully sliding the hook into the designated slot and lowering the balls into the grooves to allow the springs to apply the preload. While this attachment concept could feasibly be used, complicated design, construction, and assembly procedures preclude the usefulness and novelty of the design.

Magnetic Preload

The final securing solution, a magnet, is generally shied away from in traditional industrial environments due to their tendency to be brittle and pick up ferritic scraps. However, the simplicity and utility of the magnet design superseded these drawbacks for this metrology application. Magnetic preload has successfully been used previously for a metrology application by Federal Products Corporation. In patent 4,574,635, Federal Products used a magnetically preloaded kinematic coupling to secure and support the stylus arm of a surface finish and contour scanner.

Several different magnet types and locations could be used to provide preload for the sensor unit. For the prototype designs, a samarium cobalt disc magnet with 35 Newtons of force was chosen to secure the unit to the robot, but the magnetic force is minimized to keep the Hertz contact stress under 50% of the material limit. CAD and prototypes of this design are shown in Figure 3.13, Figure 3.14, and Figure 3.15. The magnet is placed at the

Figure 3.13   Threaded Magnet Unit

center of the coupling circle to evenly provide preload force at each of the ball to groove contacts. To allow some customization of preload force, the magnet was epoxied to a threaded fixture that allowed for a range of motion of several centimeters. Another modification to the prototype design was to include a cylindrical recess at the center of the coupling grooves to accept the magnet unit. As an additional security feature, a safety cable was added to the final magnet design to prevent the sensor unit from falling large distances.
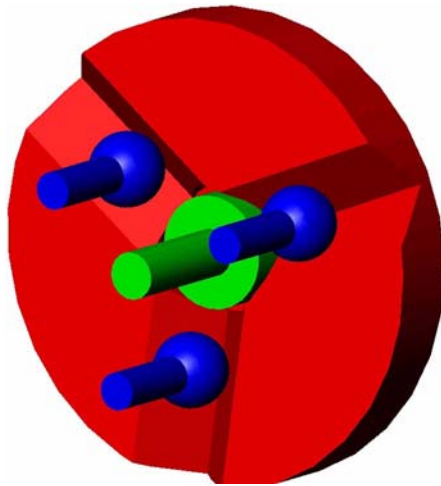
Figure 3.14   Balls and Magnet Coupled   **Figure 3.15**   Sensor Unit Plate
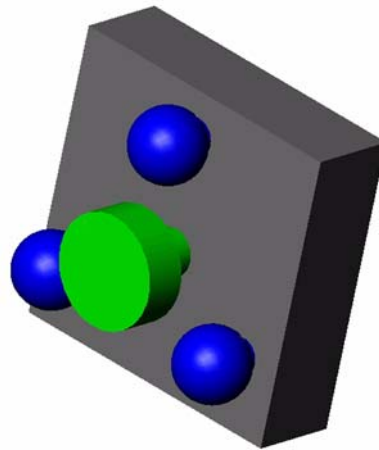
3.2.3 Coupling Location

In addition to the main functional requirement, a side goal was to attempt home position recalibration without removing the tool from the flange. This would greatly reduce the time required to perform the measurements and possibly allow for additional measurements to be performed. By changing the coupling location, major changes to the critical features of the flange could also be avoided.

Flange Edge

One of the simplest ways to attach the "Wonder Wyler" unit to the flange without requiring tool removal is to place coupling grooves on the side of the flange, as shown in Figure 3.16. This arrangement would allow for the sensor unit to easily be placed onto the edge of the flange. During calibration, the axis six joint could be rotated, provided that the tool or robot structure do not interfere with placement. While this design would simplify
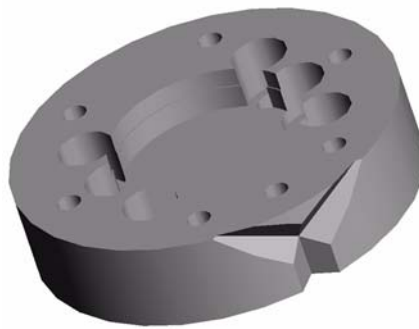
Figure 3.16   CAD Model of Flange with Edge Grooves

the use of the sensor unit, the manufacturing of three grooves on the edge of a cylinder would be difficult and costly. In addition, the device may interfere with the tool and robot structure.

"Ping Pong Paddle" Design

To avoid manufacturing issues inherent to the edge grooves, an additional design concept was generated to add a ping pong paddle shaped interface plate between the tool and flange. The main new feature of the plate is an arm, or the handle of the paddle, protruding from the side of the flange. Grooves could easily be cast or machined into the front or rear surface of the arm section to allow for coupling of the sensor unit without interfering with the robot structure or tool. Figure 3.17 and Figure 3.18 show the two possible configurations of the ping pong paddle design with sensor unit attached. To use the interface plate,
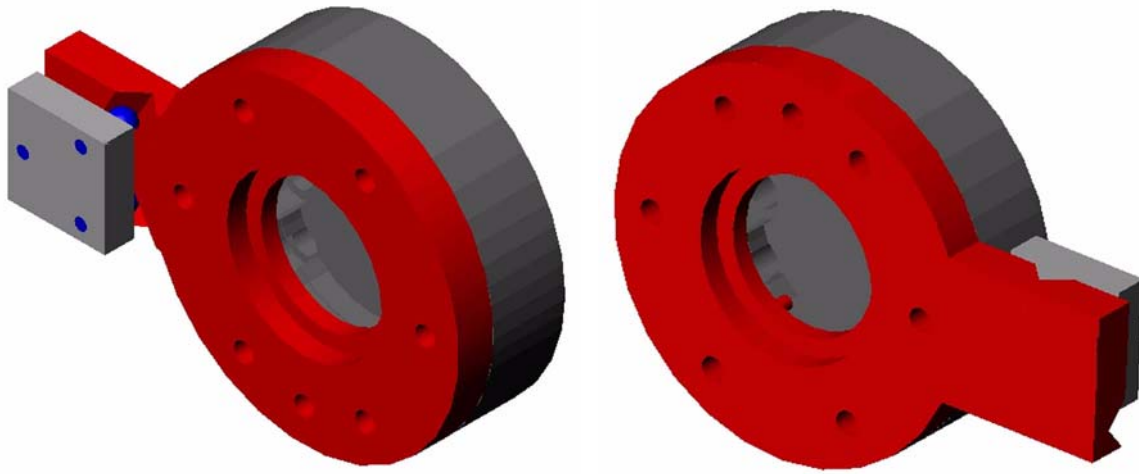
Figure 3.17   Paddle Flange Plate with Sensor Unit on
Front Mount

Figure 3.18   Paddle Flange Plate with Sensor Unit on
Rear Mount

two separate three pin couplings would attach the interface plate to the flange and the tool
to the interface plate. Another possibility is to replace the existing flange with a ping pong
paddle shaped flange, which removes the stacked couplings. However, this concept was
discarded as the arm could interfere with the robot structure at extreme positions of the
last two axes as well as interfere with objects in the robot's workspace.

3.2.4 Dynamic Axis 1 Application

The final major concern for designing the couplings for the sensor unit was the measure-
ment of the axis 1 rotation. Since the joint axis is parallel to the gravity vector, rotation of
the joint with the sensor unit mounted anywhere on the robot will not cause any deviation
in the measurement of axis rotation. Typically, this sort of measurement is performed with
a scale mounted on the edge of the cylindrical axis or a rotary encoder. Engineers at ABB
developed several solutions to measure the axis rotation, including a mechanical fork and
a hinged plate. The mechanical fork operated as merely a physical stop for the robot, while
the hinged plate method combined a physical transfer with the measurement features of
the sensor unit. To measure the rotation of the axis, a kinematic linkage transfers the rotary

motion to a tilt of the sensor unit in a measurable direction. However, these designs were not accurate enough for the measurement requirement.

As an alternative design, Torgny Brogardh of ABB suggested a new concept called the "dynamic V-groove" variation on the standard coupling. Mounted inside the cube, the two inclinometers measure the roll and pitch angles with respect to the gravity vector. The sensor unit is placed on the "dynamic V-groove," shown in Figure 3.19, which converts the
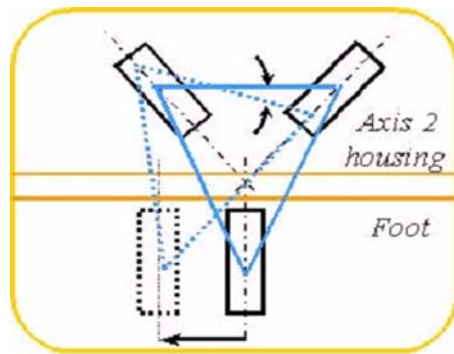
Figure 3.19 Schematic of Dynamic Groove **Figure 3.20** Dynamic Groove Prototype

axis rotation parallel to gravity to a rotation that can be measured by the inclinometers. Furthermore, the design of the groove-sphere interface causes large inclinometer measurements from small axis motions, resulting in improved calibration accuracy. This is particularly important for larger robots where a small angular error is dramatically magnified at the robot flange resulting in large positioning errors. During the design of the dynamic coupling, a major concern was that the coupling would remain stable throughout the full motion of the device. However, the required working range of the relative motion was sufficiently less than required to cause instability. A prototype of the dynamic groove was created to check the theoretical geometry checks for stability. As shown in Figure 3.20, the two coupling halves can be moved relative to each other in two directions without causing instability. To ensure that the dynamic groove plates would be compatible with the

robot geometry, a CAD model of the complete system was created as shown in Figure 3.21.
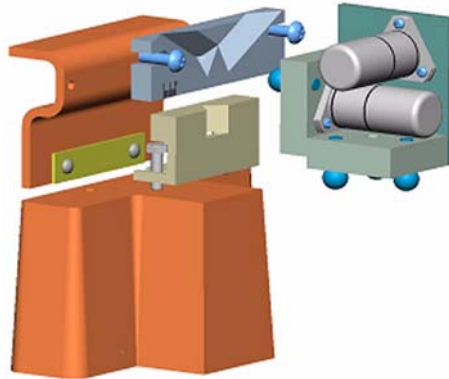
Figure 3.21   CAD Model of Dynamic V-Groove System

3.3 Physical Prototypes

In order to test out the functionality of the Wonder Wyler unit, two prototypes were constructed. The first prototype consisted of several plates bolted together, while the second prototype is a one piece, high quality machined part. The second prototype was constructed by ABB and represents the final product with only minimal changes.

3.3.1 First Prototype

Description of Prototype

The first prototype follows closely with the design development description above and consists of an open cube structure of three plates. One side plate and the bottom plate have three half inch tooling balls press fit in the coupling triangle, with a coupling circle radius of 20 mm. At the center of the coupling triangle, the threaded magnet unit is mounted in a threaded hole to provide the 35 Newton preload. These prototypes were manufactured with tolerances on the order of 0.01 mm in tool steel. For connection to the flange, a grooved insert plate was made with a sliding fit. Additional grooves for the dynamic V-groove plates and other attachment plates were manufactured at ABB and attached to

existing bolt holes. To avoid lengthy alignment of the groove plates, all measurements using the initial prototype were taken relative to the first measurement to ascertain the effect of only the ball and groove coupling and disregard the relative mounting of the groove to the robot. Figure 3.22 and Figure 3.23 show the completed Wonder Wyler sensor unit.
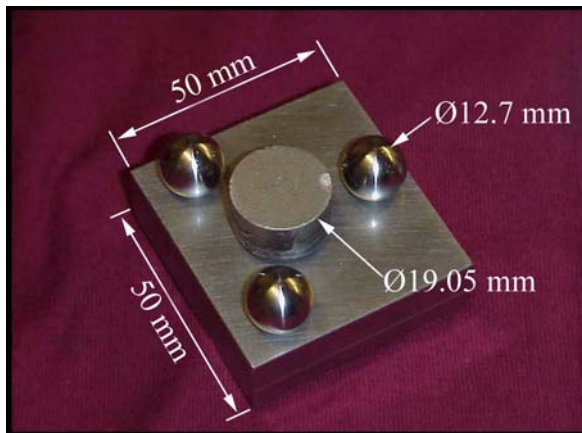
Figure 3.22   Side Plate of Sensor Unit

Figure 3.23   Complete Sensor Unit

Testing and Measurement

During testing, the sensor unit was placed on each coupling mount and each axis was moved until the sensors reported the predefined value. Several repetitions of the measurement process provided repeatability of the home position between 0.15mm to 0.35mm. This value represents a significant increase over the current levelling system and averages to within the required accuracy of 0.2 mm. In Figure 3.24, each mounting plate is shown along with the sensor unit in place in the grooves.
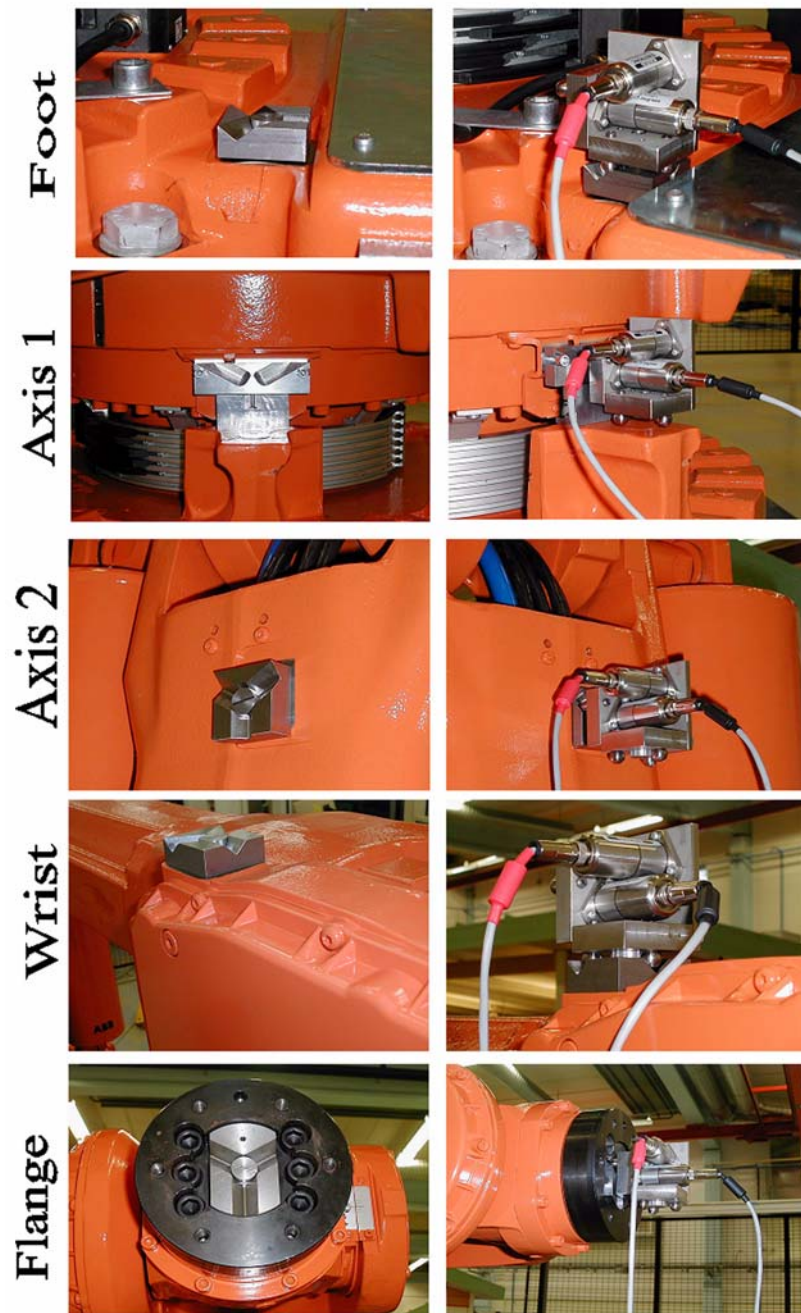
Figure 3.24   Testing of Sensor Unit

3.3.2 Final Product

The mounting repeatability of the kinematic coupling interface offers micrometer accuracy for both horizontal and vertical placements. However, error still remains within the sensor unit greater than the desired 0.2 mm recalibration error, due to variation between individual cubes caused primarily by machining tolerances of the three cube surfaces. This final issue is addressed in the completed design of the product prototype shown in Figure 3.25. To remove the inaccurate assembly of the separate plates, a single piece of

Figure 3.25   Final Prototype of Sensor Unit

Aluminum is used as the chassis for the cube. Only three outer surfaces are required to be accurate hence enabling the entire cube to be machined in a single pass with an NC milling machine. Furthermore, the mounting of the sensors on the outer surface of the cube reduces the size of the structure to approximately that of a credit card, reducing weight and allowing the cube to be used in robots with smaller accessible calibration areas. The product prototype is integrated with existing large robots through an add-on kit wherein the V-groove plates are permanently bolted to the robot structure. For optimal cost and performance V-grooves are directly machined into the robot structure on newer robot models.

The results of recalibration tests satisfy the original specifications, revealing an error of 0.2mm, which represents a five-fold improvement on the existing system.

Chapter 4

MEDIUM SCALE DESIGN CASE STUDY: WRIST INTERFACE

4.1 Background and Problem Description

4.1.1 Background

Out of the entire line of ABB Robots, the IRB 6400R robot is one of the most versatile and popular robots, especially in the automotive industry. Common uses include painting, assembly, welding, material handling, and other industrial tasks. With full six degree of freedom control, the 6400R is capable of positioning and orienting a 200 kg tool at a maximum speed of 2 to 3 meters per second. While carrying a 150 kg load, the IRB 6400R can maintain 1 mm accuracy along the path while traveling at 1 m/s or 0.1 mm point to point accuracy. To achieve this level of accuracy, each robot is calibrated before it leaves the factory. The optimum calibration is performed by measuring a complete set of robot poses using a Leica LTD500 Laser Tracker System, a 3D tracking interferometer. These measurements are then used to develop a set of error parameters to describe the errors between the measured locations and the locations predicted from the robot's kinematic model. By integrating these parameters in the robot's control system, the position and orientation errors can be actively corrected for a given tool load.

Over time, the errors present in the robot system may decrease due to a noticeable change in robot performance or the replacement of a critical structural component. Down time of several hours of maintenance would be required to perform additional calibration neces-

Figure 4.1   ABB IRB 6400R Robot   **Figure 4.2**   Wrist Unit of IRB 6400R
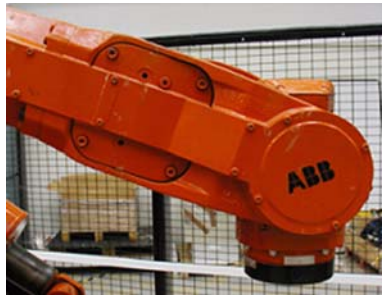
sary to restore the robot to optimal performance. In many industries, down time of several hours can shut down an entire assembly line, entailing many thousands of dollars of lost work. Often, some manufacturers will remove an entire robot rather than replace the major component online and recalibrate.

One of the more commonly replaced components on a robot is the robot wrist, which is a large component housing the motors and mountings for the last two axes. A wrist replacement can require approximately a half hour to perform the physical operations, while the subsequent calibration requires approximately two to eight hours to restore the robot to reasonable accuracy. To reduce the required calibration time, kinematic couplings could be incorporated in the interface between the robot wrist and the upper arm of the main structure. Since the coupling will be inherently more repeatable, the location of robot's tool flange will deviate less from the pre-replacement location. Instead of performing a lengthy calibration of a hundred or more poses, a much shorter calibration can be performed to restore the robot's accurate performance. For a full description of the repeatability and accuracy of a coupling, the effects of both repeatability and interchangeability

must be addressed. The issue of interchangeability between wrist individuals is essentially an issue of tolerances and manufacturing and will not be discussed in this study.

4.1.2 Problem Description and Functional Requirements

Although kinematic couplings are used regularly in many precision engineering application, they have rarely, if ever, been applied to industrial robotics. For kinematic couplings to work in this setting, a new range of issues must be addressed including high loads, installation issues, and applicability. To develop experience with these issues, several kinematic coupling designs will be created for the IRB 6400R robot to introduce the concepts for future implementation in ABB robots. The end product of this work is to develop experience using kinematic couplings in industrial robotics and to transfer this experience to the engineers at ABB. Design of the 6400R couplings is guided by the following functional requirements:

1. Improve the repeatability of a wrist replacement on the 6400R robot.

2. Minimize physical changes to wrist structure.

3. Minimize or prevent any reduction in structural performance of wrist interface.

4. Minimize cost of new wrist design.

Initially, the goal of the new interface design was to reduce the existing wrist replacement error of 1.0 mm. During testing, a single wrist interface revealed that replacement repeatability of 0.1 mm could be achieved with the existing interface. However, this repeatability may not be indicative of the performance of all wrist interfaces, as only a single interface was measured. Since these measurements may indicate that the wrist interface performs much better than originally speculated, the target for design repeatability was to render the replacement of a wrist indistinguishable to the measuring system. The Leica interferometer system that is currently used for calibrations at ABB is capable of measur-

ing 10 μm per meter, which translates to a measurement accuracy and design target of about 20 to 30 μm.

4.2 Design Development and Construction

The strategy for achieving these goals is to implement a series of adapter plates that could be fixed to the existing wrist interfaces and that allow the new couplings to be safely tested. The new interfaces to be attempted are the standard kinematic coupling using canoe ball elements and a three pin coupling. Quasi-kinematic couplings were not implemented and tested due to time and financial constraints.

4.2.1 Existing Wrist Coupling

As shown in Figure 4.3 and Figure 4.4, the existing wrist coupling consists of rather complex implementation of a pin coupling. Primary coupling features include four highly tol-
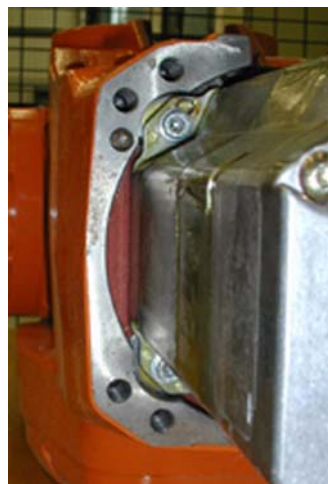
Figure 4.3 Existing Coupling Features on Arm   **Figure 4.4** Existing Coupling Features on Wrist

erances control tabs on the robot structure that interface with similarly toleranced control surfaces on the wrist. While the control features constrain two translational degrees of freedom in the interface plane, an additional control pin is required to constrain the third

degree. Surface contact across the interface plane constrains the remaining degrees of freedom. Across the interface, forces and moments are opposed using eight bolts normal to the interface and friction coplanar to the interface. As extremely high loads are carried by the interface, friction between the interface surfaces is not sufficient to support the moments so additional dimpled friction plates are included at the interface, as shown in Figure 4.5.

Figure 4.5   Friction Plate at Wrist Interface

TABLE 4.1   Loading Cases at Wrist Center for ABB IRB 6400R

	Normal Operation (min, max)	**Emergency Braking Load (min, max)**
X - Force (kN)	-13.7, 3.0	-13.4, 28.4
Y - Force (kN)	-12.9, 9.8	-23.7, 29.9
Z - Force (kN)	-12.8, 13.1	-30.6, 28.1
X - Moment (kN-m)	-2.8, 5.4	-14.1, 8.6
Y - Moment (kN-m)	-8.7, 5.7	-8.2, 20.4
Z - Moment (kN-m)	-9.5, 7.4	-31.2, 29.3

Table 4.1 lists the forces and moments on the interface for the normal operation and emergency braking conditions as predicted by simulations. The minimum and maximum values given are for the worst possible conditions in the specified direction and would never occur simultaneously.

As mentioned above, the repeatability of an existing wrist replacement is estimated by ABB to be 1 mm at the tool flange, while the measured repeatability of a wrist individual is 0.1 mm. Due to the nature of the coupling, both interchangeability and repeatability are limited by the tolerances of the interface geometry, which are approximately ±0.010 to ±0.100 mm. The application of kinematic principles will decrease the dependence of repeatability on tolerances.

4.2.2 Kinematic Coupling

The first of the two new coupling interfaces is the standard kinematic coupling. Because of the high loading case occurring at the wrist, canoe ball elements will be used to improve performance. The canoe balls used on the wrist were originally designed for a separate project and ordered in bulk to reduce the price. Consequently, some limitations are placed
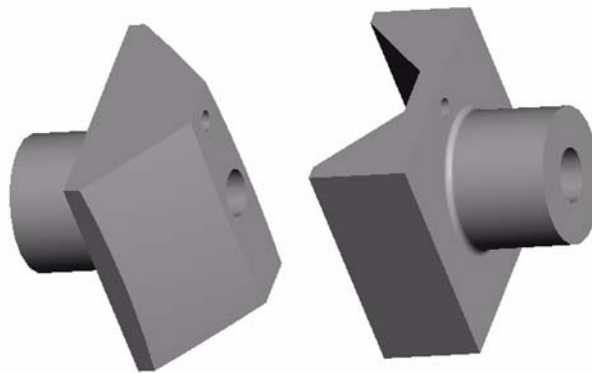
Figure 4.6   Canoe Ball and Groove Elements

on the design, although their load capacity is sufficient for the wrist. Basic material properties for the canoe balls are 420 Stainless steel and hardened to 50 - 55 Rockwell C with surface finish as ground. Basic dimensions are radius of 250 mm for the canoe surfaces and an equivalent ball diameter (contact point to contact point) of 30 mm.

In Figure 4.7 and Figure 4.8, an assembled model and an exploded model of the CAD geometry are shown. The components are ordered from left to right as follows: interface
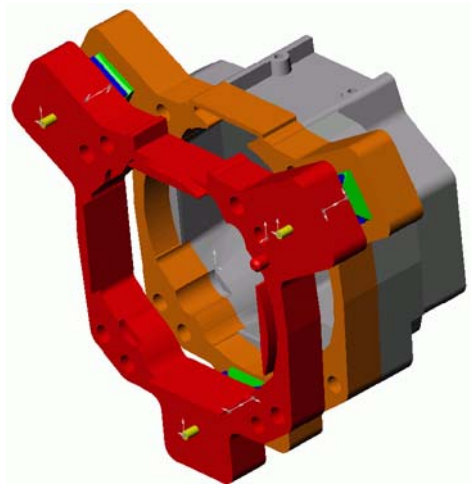
Figure 4.7 Wrist Interface Assembly   **Figure 4.8** Exploded Wrist Interface Assembly
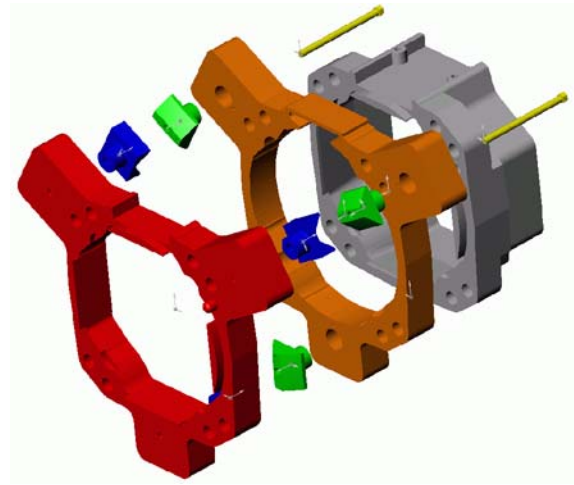
plate to wrist, groove elements, canoe ball elements, interface plate to arm, arm interface, and preload bolts. Interface plates are made of 17-4 ph Stainless Steels, which are relatively easy to machine while providing high strength, high hardness, and excellent corrosion resistance.

General Design Concerns

Because of the restricted space available on the wrist interface, placement of the coupling becomes a major problem to overcome. For the prototype design, this problem is bypassed by creating extra tabs that protrude from the wrist interface area. These tabs were sized quite large to prevent any bending of the interface plates during testing and operation. In future revisions of this design, the canoe balls could be incorporated as integral features to the wrist interface, especially since large protrusions from the wrist are undesirable in any environment. Furthermore, the gap between the two interface plates must be sealed for use in any industrial environment where grease, oil, debris, and other contaminants could be introduced to the internals of the robot arm. Some form of interface seal or a quasi-kinematic coupling could be used.

One concern for using interface plates to test the coupling prototypes is the possibility of relative motion between the components. If relative motion of one plate to the robot structure were to occur, repeatable results would be impossible to obtain. To prevent undesired motion, each interface plate will be secured to the corresponding robot interface with four M12 bolts. Four additional M12 bolts will be placed through the entire assembly as an emergency security precaution against wrist damage if the preload bolts or interface plates fail.

Similarly, relative motion between the coupling elements and the interface plates is undesirable. To prevent motion, the coupling elements are press fit into corresponding holes on the interface plates. Rotation about the element shank is prevented using a press fit dowel pin with a matching hole on the element.

Preload

Preload for the kinematic couplings was determined based on the weight of the wrist only, assuming the wrist is hanging from the arm at a 45° angle with respect to ground. Normal operation forces and emergency stop forces were not considered, as ABB engineers limited testing of the wrist prototypes to a static replacement to prevent the chance that the robot might be damaged. Based on an estimate of wrist mass of 100 kg, it was determined that 10 kN of preload through each ball center was necessary to set the coupling. Because of the small size of the coupling elements, the maximum size bolt is limited to an M6. Using the procedures documented in Bickford and Nassar, this preload translates to a required 15 N-m torque on a class 12-9, M6 bolt, which ensures that stress in the bolt remain 90% of the yield stress. No additional preload can be applied on these coupling elements using these bolts without risking bolt failure.

Contact Stress

Under the preload and weight of the wrist, the kinematic couplings exhibit contact stress at an acceptable level of less than 40% of the allowable stress. Contact stresses increase only slightly if the normal operation forces are applied to the coupling elements; however,

emergency braking loads will cause high contact stresses and reversal of contact forces. The mathematics describing performance of this coupling are included in Appendix A.

Stiffness

Since one of the main functional requirements is to minimize any reduction in performance of the new wrist interface, joint stiffness must be investigated. To perform a relative comparison of stiffness, a series of finite element models were created using the SDRC IDEAS software package. Results of simulations for four models are shown in Table 4.2. For each model, two separate simulations were performed to analyze the stiff-

TABLE 4.2 Deflection Results for FEA Simulations

Model Name	Y-Deflection (um)	Z-Deflection (um)
Straight Beam	8.11	7.24
Bolted Interface	8.88	8.02
New Interface - Flexure Approximation	44.3	58.1
New Interface - Modulus Approximation	34.4	47.7

ness variance in different directions. Results indicate the deflection resulting from a 1000N force in either the Y or Z direction as shown in the corresponding model figures below. First, two simulations were performed to determine the stiffness properties of the arm geometry as if it were a straight beam and with the existing interface. Relatively similar deflections occurred in both the Y and Z directions for both models, indicating that the bolted interface performs almost like a single, contiguous piece.

In order to accurately describe the stiffness of the canoe ball interface, two simulations were performed with separate approximations of the interactions between the canoe ball and groove elements. The first approximation uses hinge flexures to simulate the stiffness of the new interface as predicted by the Hertzian contact mechanics in Appendix A. In Figure 4.10, the flexure geometry is determined to be a 35 mm cube with cutout radius of 17.5 mm. Instead of geometrically changing the stiffness properties, the second approxi-
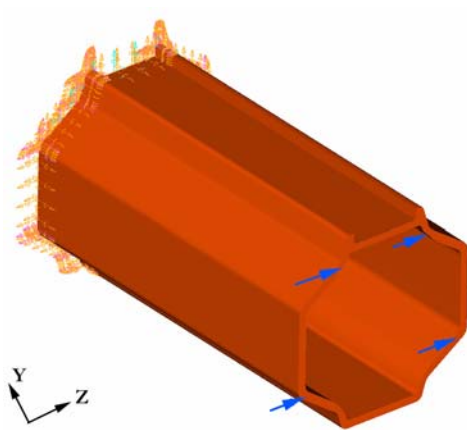
Figure 4.9 FEA Model for Straight Beam
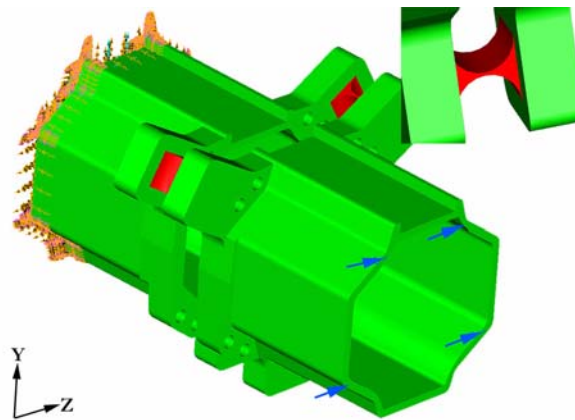
Figure 4.10 FEA Model for FEA Approximation

mation applies an altered Young's modulus to a 35 mm cube to simulate the predicted stiffness change. In both approximations, each canoe ball - groove interface is replaced by one of the approximate geometries. Mathematics necessary to design the hinge flexures and the material change are included in Appendix C and FEA plots are presented in Appendix D. Overall, both approximations illustrate significant reductions in the stiffness of the interface from the original design. To fully understand the effect of the stiffness reductions, the changes must be incorporated into the robot kinematic and dynamic models to determine whether or not undesired performance will result.

4.2.3 Three Pin Coupling

The second coupling to be tested on the wrist interface is the three pin coupling, a form of the planar kinematic coupling. Similar to the design of the three pin flange interface in Chapter 3, the three pin wrist interface uses three pins with a properly applied preload to constrain the three degrees of freedom in the interface plane and surface contact to constrain the remaining degrees.

General Design Concerns

One of the benefits of using the three pin coupling on the wrist is the ease with which the existing wrist coupling geometry can be adapted into the more deterministic design. The
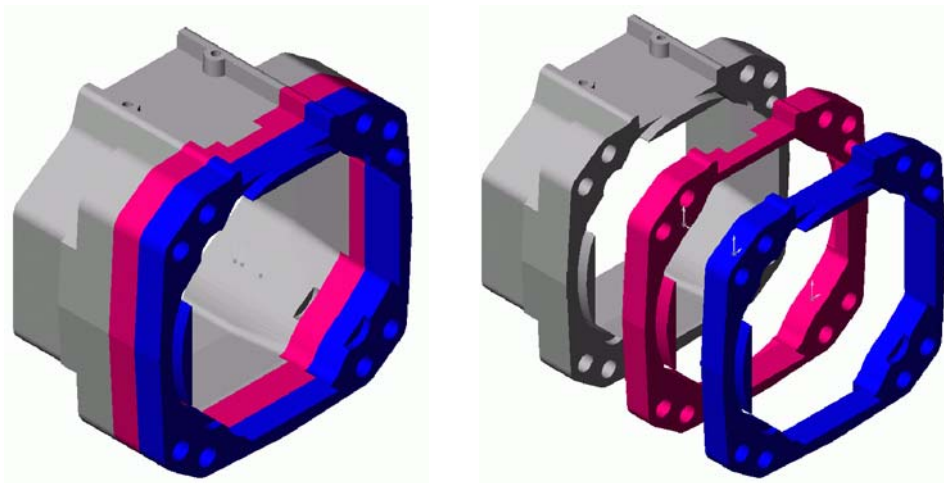
Figure 4.11   Three Pin Wrist Assembly **Figure 4.12**   Exploded Three Pin Wrist Assembly

existing coupling consists of a control pin and four cylindrical control surfaces that are coradial and concentric. By removing two of the control surfaces, all necessary features are present for the positive coupling half. On the mating interface, the control recesses corresponding to the remaining control surfaces can be machined out to create flat surfaces for line contacts with the two control surface pins. Due to the large radius of these control surface pins, they possess high load carrying capacity using the same phenomenon as the canoe ball elements. The final mating feature is a specially designed pill shaped hole that accepts the control pin and allows for a singular line contact along its circumference. Figure 4.13 shows a cut-away prototype of the two coupling interfaces to illustrate the general geometry. To check the design for success, a force and moment balance on the interface is performed using the free body diagram in Figure 4.14.

Preload

When using the three pin coupling, two separate preloads are required to properly set the coupling. The first preload occurs in the plane of the coupling and is used to set the coupling against the interface friction and any in-plane static loads. Since the coupling is only subjected to the weight of the wrist, the in-plane preload is not required to apply any constraining load against the wrist weight. In-plane preload is applied using a M6 set screw
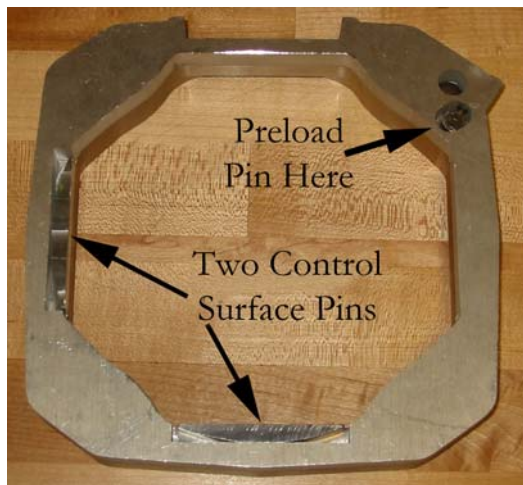
Figure 4.13   Basic Three Pin Geometry   **Figure 4.14**   Free Body Diagram for Three Pin
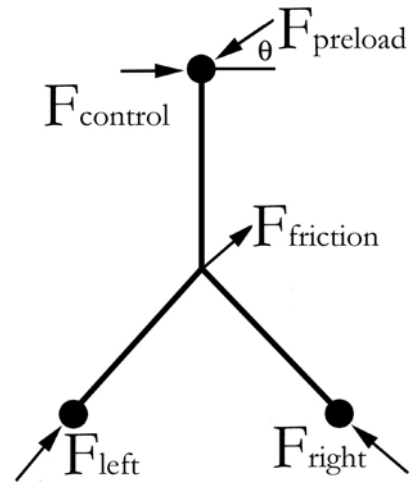
with a brass tip. By including the brass tip, some compliance is added to the preload bolt to prevent overconstraint. The exact in-plane preload force could not be calculated as the coefficient of friction for the interface was unavailable. For the second preload, bolts normal to the interface plane close the coupling and apply the load carrying preload. The weight of the wrist and small dynamic forces caused by small moving the robot to any measurement positions will be held four M12 bolts threaded into the robot structure.

Stiffness

One of the main benefits of the three pin coupling is that no reduction in stiffness occurs in comparison to the original coupling. On the existing interface, the only load carrying features are the perpendicular bolts, frictional plates, and surface area, all of which remain on the three pin coupling. The changes between the two couplings occur on control features that are used for alignment purposes only and have no structural properties. Estimates of

three pin coupling stiffness would be similar to those for the bolted joint shown in Table 4.2.

4.3 Physical Prototypes

As mentioned previously, each wrist prototype consists of two interface plates made of 17-4 PH stainless steel. Negative features of the robot structure's interfaces are machined into the appropriate side of the coupling to easily allow installation of the plates. Four M12 bolts secure each of the plates to the respective robot structure. For the canoe ball and groove coupling, the coupling elements are press fit into blind holes and are pinned to prevent rotation about the shank. The three pin coupling has features as machined and requires no additional assembly. The prototypes are shown in Figure 4.15 and Figure 4.16 as single units attached to the robot and as coupled.

Testing System and Procedure

The testing setup for the ABB IRB 6400R consists of a full robot cell, including robot, control system, and a Leica LTD Laster Tracker. To measure the effect of wrist replacement, a cat's eye retro-reflector was attached to the tool flange. The retro-reflector allows the laser tracker to follow the location of the robot while measuring the distance between the robot and laser head and the three angles of the laser head. In the Leica computer controls, these measurements are combined to present the X,Y,Z coordinates of the reflector with accuracy of 10 μm per meter. Corrections are made in the controller using a temperature measurement to correct thermal errors in the measurement system.

To measure the repeatability, each type of coupling was installed on the existing interfaces then coupled together with the robot powered down. Upon powering the robot, measurements were taken at five points throughout the robot's working space, as shown in Figure 4.17. This procedure is contrary to the initial assertion by ABB engineers that the robot could not be moved with the new couplings in place due to possible safety risks. However, measurements of the robot at different points in the workspace were very
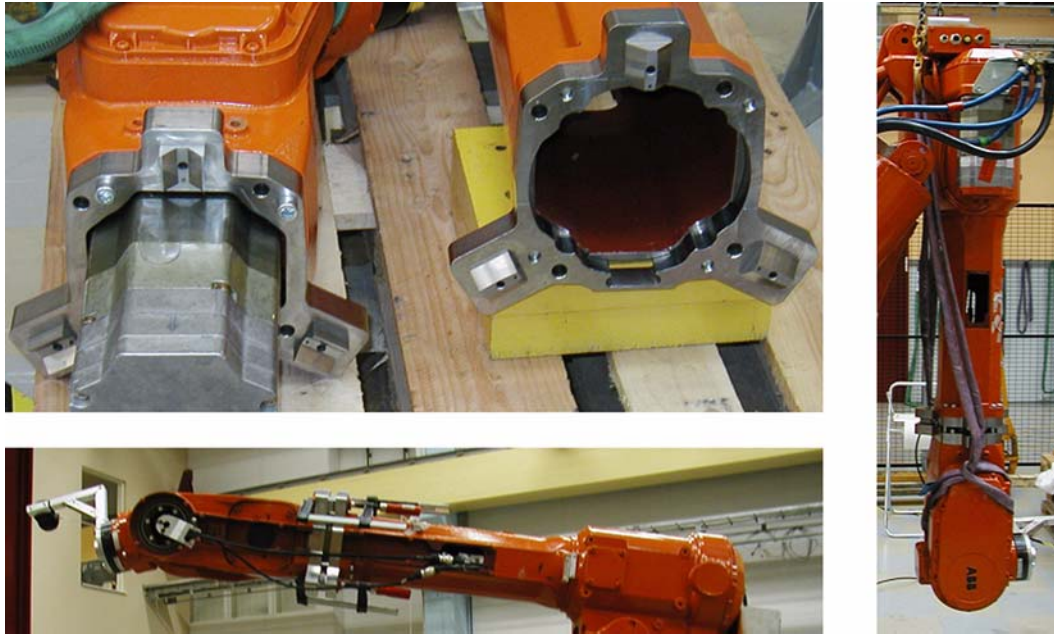
Figure 4.15   Canoe Ball and Groove Coupling Prototypes

Figure 4.16   Three Pin Coupling Prototypes
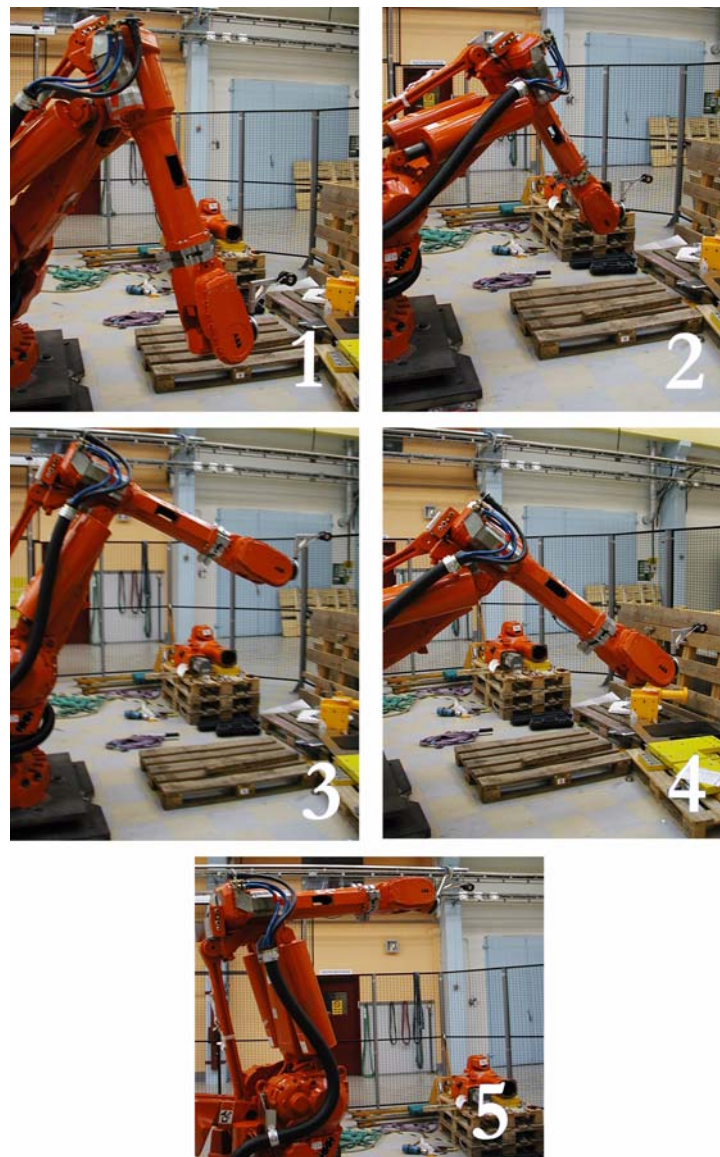
Figure 4.17   Fives Positions of Robot in Dynamic Test

instructive on the performance of an under designed coupling. Note that in positions three and five, the angle of the wrist deviates significantly from the position where the arm is perpendicular to the ground. As the original design of the canoe ball and groove coupling was limited to this position only, optimal performance could not occur in these significantly different positions. Additional measurements were taken without moving the robot to assess the static repeatability of the coupling. Furthermore, two separate installation

positions were tested to investigate the effect of the initial relative position of the couplings. The first position is the standard wrist replacement position used for the IRB 6400R, shown in Figure 4.18, while the second position places the arm and wrist parallel to gravity, shown in Figure 4.19.
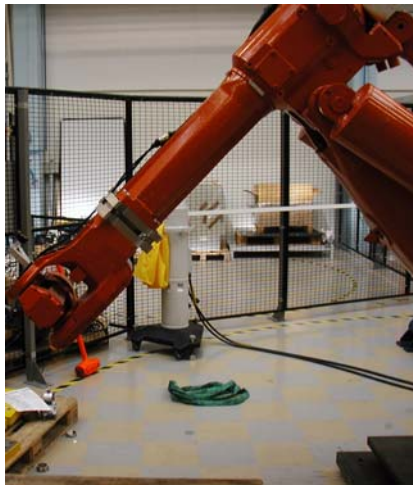
Figure 4.18   45° Installation Position   **Figure 4.19**   90° Installation Position

In both positions, installation is assisted using a crane to grossly position the wrist. Fine positioning is performed by evenly tightening the peripheral bolts until the contact surfaces touch. Using stepped torquing of 10%, 50%, and 100%, the proper preloads are applied to the three preload bolts on the canoe ball and groove coupling. The peripheral bolts are tightened to finger tight to provide security against wrist separation if the preload bolts fail. Due to underestimation of the wrist weight and the presence of unexpected dynamic forces, extra preload was required to set the coupling in most positions. Two methods were employed to apply additional preload: loading applied through peripheral bolts in parallel with the preload bolts and clamps applied in series with the preload bolts. The lower left image in Figure 4.15 shows the clamps installed along the preload bolts.

For the installation of the three pin coupling, the peripheral bolts are tightened to still allow movement along the interface plane. The in-plane preload is then applied to set the

coupling. During testing, a torque wrench was not available with the proper attachment for the in-plane preload bolt. Therefore, a repeatable in-plane preload was not possible for these experiments. The preload bolt was tightened until the coupling plates move into place, then the peripheral bolts are tightened to 120 N-m as typically performed during installation. After two wrist replacements, noticeable deformation of the brass tip on the preload bolt was observed and the bolt was exchanged every two wrist replacements. Friction plates are also placed on the interface during coupling for maximum load capacity. After the first series of measurements, some change occurred in the coupling, causing a significant decrease in the repeatability. It is surmised that damage occurred between the control pin and receptacle due to the creation of scratches and marks in the interface region. When exchanging the wrist in the 45° position, a large moment is incurred about the lifting straps. This moment creates motion between the wrist relative to the arm, causing the precision interface features to scrape each other and remove the deterministic relationship. Future testing and implementations should be performed in the 90° position to prevent damage.

4.3.1 Results

The easiest way to present the results is show the progression of measurement results to illustrate the changes caused by the different variables . Figure 4.20 shows a table of the different measurements of average point to point repeatability, progressing in an improved understanding of installation procedures. Table 4.3 shows the results with matching conditions for each measurement in Figure 4.20.
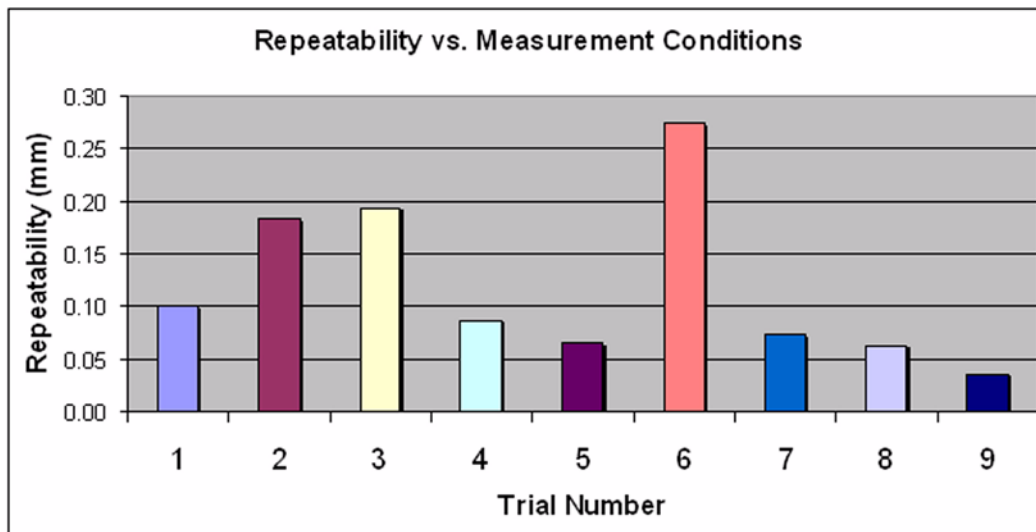
Figure 4.20   Average Repeatability vs. Measurement Conditions for Canoe Ball and Groove Coupling

TABLE 4.3   Canoe Ball and Groove Coupling Results

Measurement	Installation Position	Additional Preload	Measurement Type	Bolting Procedure	Average Point to Point Repeatability
1	Original Interface				0.1011 mm
2	45°	0 N-m	5 pt.	Plain	0.1834 mm
3	45°	15 N-m	5 pt.	Plain	0.1940 mm
4	45°	50 N-m	5 pt.	Plain	0.0872 mm
5	45°	75 N-m	5 pt.	Plain	0.0662 mm
6	45°	120 N-m	5 pt.	Plain	0.2749 mm
7	90°	0 N-m	5 pt.	Refined	0.0736 mm
8	90°	Clamps	5 pt.	Refined	0.0626 mm
9	90°	Clamps	Static	Refined	0.0366 mm

Preload listed in the additional preload column is in addition to the 10 kN preload applied using the preload bolts. Numbers listed correspond to the preload torque applied to the peripheral bolts, while the word clamps indicates the unmeasured clamp load. In the fourth and fifth series of measurements, the increase in peripheral preload improved repeatability, however, the increase to 120 N-m in the sixth measurement created a suffi-

ciently large bending moment to cause relative motion between the coupling elements. While adding preload in parallel with the preload bolts is undesirable due to the bending moments, the measurements with additional preload applied in series improved the repeatability without undesirable effects. Since the size of the preload bolts could not increase, the use of clamps increased the preload applied and improved repeatability. Clamps are not a desirable addition to the design of the robot, so future coupling designs require more flexibility in preload application. In addition to preload changes, noticeable improvements in repeatability coincided with improved bolting procedure and installation position. The main benefit of performing a wrist installation in the 90° position is that all forces on the coupling are parallel to the installation direction. Non-parallel forces induce rotations of the coupling, causing quite different initial positions of the elements and different force distributions across the elements.

For the three pin coupling, only three measurement sets were available due to the damage incurred. Figure 4.21 shows the average point to point repeatability results for the three pin coupling and Table 4.4 lists the conditions at each measurement.
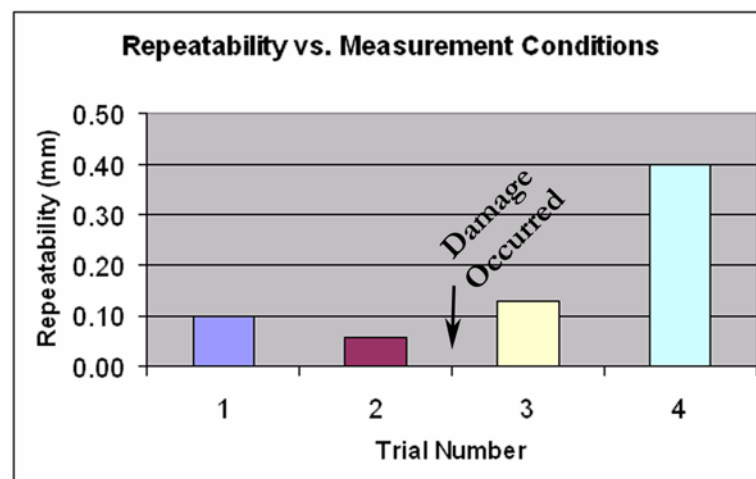
Figure 4.21 Average Repeatability vs. Measurement Conditions for Three Pin Coupling

TABLE 4.4   Three Pin Coupling Results

Measurement	Installation Position	Measurement Type	Average Point to Point Repeatability
1	Original Interface		0.1011 mm
2	45°	5 pt., good	0.0572 mm
3	90°	5 pt., damaged	0.1309mm
4	45°	5 pt., damaged	0.4066 mm

As mentioned earlier, the first measurements of the three pin coupling indicated potential for a significant increase in repeatability with a minimal change in the design. However, damage occurred before sufficient measurements could be taken and repeatability of the coupling became worse than the existing coupling.

Chapter 5

CONCLUSION

In this document, a overview of design theory on kinematic couplings has been presented with specific detail to the classic ball and groove coupling and the newer three pin coupling. A collection of implementation and installation guidelines are also presented for using these couplings in an industrial setting. In particular, the theory and guidelines have been directed towards design of couplings for use under high load and detrimental conditions. Proper analysis of static and disturbance forces as well as contact stress at the contact points allow for inclusion of kinematic coupling elements into these settings.

Through the application of kinematic couplings to a small scale calibration device, kinematic couplings have made an entrance into the industrial setting via a metrology application. The use of this device allows for quick recalibration of the home position of the ABB IRB 6400R robot, as well future use on other robot lines. Challenges overcome in the design of the device include developing solutions for applying preload simply and consistently, while preventing the calibration device from falling off the robot. A novel design developed is the dynamic V-groove, which allows a device perpendicular to gravity to measure a rotation parallel to gravity without developing instabilities. At the project start, a target of 0.2 mm was placed on the repeatability of the home position calibration. The final prototype maximized repeatability of the robot to device interface and minimized device manufacturing errors to successfully meet project requirements.

Through the application of kinematic couplings to a medium scale, high load interface, kinematic couplings have become a viable option for inclusion in the menu of design tools available to the industrial designer. The research presented in this thesis shows preliminary results demonstrating the improved performance provided by kinematic couplings when applied to the high load wrist interface of the ABB IRB 6400R robot. Applications of kinematic coupling theory have not been done previously on this scale. In order to present a baseline measurement of coupling design, the classic ball and groove coupling design was developed and tested on the wrist. Because of the high loads present at the wrist, canoe ball elements were used in place of standard hemispeheres to reduce contact stress while retaining repeatability. These results were compared to the existing pin joint interface and a new three pin coupling that uses elements of the existing interface to create a more deterministic coupling. In static measurements, the canoe ball coupling presented a 64% improvement in repeatability and 35% improvement in repeatability for dynamic measurements. The three pin coupling showed potential of a 44% reduction for dynamic measurement with minimal changes to the interface, however, the critical interface features were damaged during testing. Since the three pin coupling presents the most inexpensive solution, further testing is required to test the true performance of the three pin coupling.

In addition to further testing of the three pin coupling, additional investigation should proceed in several other areas, including friction reduction using coatings, long term dynamic performance, and the effect of off center loads during mounting and operation. Laboratory tests should also be performed to obtain an ideal limit for the repeatability of three pin coupling in comparison to the classic ball and groove coupling. These tests will further the concept of an accuracy design menu, allowing different couplings to be easily compared for repeatability, cost, and other factors.

REFERENCES

General Precision Machine Design

Hale, Layton C. "Principles and Techniques for Designing Precision Machines." Ph.D. Thesis, Massachusetts Institute of Technology, Cambridge, MA, 1999.

[Slocum, 1992a] Slocum, Alexander H. Precision Machine Design. Prentice-Hall: Englewood Cliffs, NJ, 1992.

Slocum, Alexander H. "Method of and Apparatus for Locating and Orientating a Part on a Gripper and Transferring it to a Tool While Maintaining Location and Orientation on the Too.l" U.S. Patent 5,711,647, January 27, 1998.

Smith and Chetwynd. Foundations of Ultraprecision Mechanism Design. Gordon & Breach Science Publishers: Montreux, Switzerland, 1992.

General Design Principles and Theory

[Beer, 1992] Beer, Ferdinand P. and Russell Johnston, Jr. Mechanics of Materials. 2nd ed. McGraw-Hill, Inc.: New York, 1992.

[Bickford, 1998] Bickford, John H. and Sayed Nassar, eds. Handbook of Bolts and Bolted Joints. Marcel Dekker, Inc.: New York, 1998.

[Blanding, 1999] Blanding, Douglas K. Exact Constraint: Machine Design Using Kinematic Principles. ASME Press: New York, 1999

[Johnson, 1985] Johnson, K.L. Contact Mechanics. Cambridge University Press: Cambridge, UK, 1985.

Mott, Robert L. Machine Elements in Mechanical Design. 2nd ed. Prentice Hall: Upple Saddle River, NJ, 1992.

Design of Kinematic Couplings

Hale, Layton C. and Alexander H. Slocum. "Optimal Design Techniques for Kinematic Couplings", Precision Engineering, 25, 114-127, 2000.

[Mullenheld, 1999] Mullenheld, Bernard. "Prinzips der kinematischen Kopplung als Schnittstelle zwischen Spindel und Schleifscheibe mit praktischer Erprobung im Vergleich zum Kegel-Hohlschaft" (Application of kinematic couplings to a grinding wheel interface), SM Thesis, Aachen, Germany, 1999.

[Slocum, 1988a] Slocum, Alexander H. "Kinematic Couplings for Precision Fixturing -- Part I: Formulation of Design Parameters", Precision Engineering, 10.2, 85-91, 1988.

[Slocum, 1988b] Slocum, Alexander H. and Alkan Donmez. "Kinematic Couplings for Precision Fixturing - Part 2: Experimental Determination of Repeatability and Stiffness", Precision Engineering, 10.3, July 1988.

[Slocum, 1992b] Slocum, Alexander H. "Design of Three-Groove Kinematic Couplings", Precision Engineering, 14.2, 67-76, 1992.

Design of Quasi-Kinematic Couplings

[Culpepper, 2000] Culpepper, Martin L. "Design and Application of Compliant Quasi-Kinematic Couplings", Ph.D. Thesis, Massachusetts Institute of Technology, Cambridge, MA, 2000.

Culpepper, Martin L. and Alexander H. Slocum. "Quasi-Kinematic Coupling and Method for Use in Assembling and Locating Mechanical Components and the Like", U.S. Patent 6,193,430, February 27, 2001.

Use of CAE in Design

Bamberg, Eberhard. "Principles of Rapid Machine Design", Ph.D. Thesis, Massachusetts Institute of Technology, Cambridge, MA, 2000.

Dimarogonas, Andrew D. Computer Aided Machine Design. Prentice Hall: New York, 1989.

Zhavi, Eliahu. The Finite Element Method in Machine Design. Prentice Hall: Englewood Cliffs, NJ, 1992.

Project Specific Resources

ABB IRB6400R Product Manual.

Leica LTD500 Product Information, http://www.leica.com.

Wyler AG Zerotronic Measurement System, http://www.wylerag.com.

[Robertson, 2001] Robertson, A., Slocum, A., Willoughby, P. "Precision Robot Calibration Using Kinematically Placed Inclinometers." Proceedings of 2001 ASPE Conference, p 229 - 232.

Appendix A

FORMAL KINEMATIC COUPLING MATHEMATICS IN MATHCAD

Describe Basic Geometry of Coupling

General Coupling Info:

$D_{coupling} := 260mm$ Diameter of circle where grooves and balls are located

$F_{preload} := -10000N$ Preload applied through center of each ball and groove, off center loading should be defined below

Where should error be reported at?

$x_{err} := -250mm$

$y_{err} := 0mm$

$z_{err} := 500mm$

Groove 1

$\theta_1 := 0deg$

$R_{g\_1} := 1\cdot10^6 \ m$

$groove1 := 90deg$

$E_{g1} := 206.8\cdot10^9 Pa$

$Hertz_{g1} := 1.72\cdot10^9 Pa$

$\upsilon_{g1} := .29$

Groove 2

$\theta_2 := 240deg$

$R_{g\_2} := 1\cdot10^6 \ m$

$groove2 := 90deg$

$E_{g2} := 206.8\cdot10^9 Pa$

$Hertz_{g2} := 1.72\cdot10^9 Pa$

$\upsilon_{g2} := .29$

Groove 3

$\theta_3 := 120deg$

$R_{g\_3} := 1\cdot10^6 \ m$

$groove3 := 90deg$

$E_{g3} := 206.8\cdot10^9 Pa$

$Hertz_{g3} := 1.72\cdot10^9 Pa$

$\upsilon_{g3} := .29$

Ball 1

$D_{eq\_b\_1} := 30mm$

$R_{b\_min\_1} := 250mm$

$R_{b\_maj\_1} := 250mm$

$E_{b1} := 206.8\cdot10^9 Pa$

$Hertz_{b1} := 1.72\cdot10^9 Pa$

$\upsilon_{b1} := .29$

Ball 2

$D_{eq\_b\_2} := 30mm$

$R_{b\_min\_2} := 250mm$

$R_{b\_maj\_2} := 250mm$

$E_{b2} := 206.8\cdot10^9 Pa$

$Hertz_{b2} := 1.72\cdot10^9 Pa$

$\upsilon_{b2} := .29$

Ball 3

$D_{eq\_b\_3} := 30mm$

$R_{b\_min\_3} := 250mm$

$R_{b\_maj\_3} := 250mm$

$E_{b3} := 206.8\cdot10^9 Pa$

$Hertz_{b3} := 1.72\cdot10^9 Pa$

$\upsilon_{b3} := .29$

Is ball major radius along groove axis? If yes, costheta = 1 or costheta = π if not.

$theta := 0deg$

$costheta := cos(theta)$

$costheta = 1$

More Detailed Preload Forces:

$F_{px\_1} := 0N$ $F_{px\_2} := 0N$ $F_{px\_3} := 0N$

$F_{py\_1} := 0N$ $F_{py\_2} := 0N$ $F_{py\_3} := 0N$

$F_{pz\_1} := F_{preload}$ $F_{pz\_2} := F_{preload}$ $F_{pz\_3} := F_{preload}$

Location of Preload Forces (Default is to center of balls, can be changed below):

$x_{p\_1} := \dfrac{D_{coupling}}{2} \cdot \sin(\theta_1)$ $x_{p\_2} := \dfrac{D_{coupling}}{2} \cdot \sin(\theta_2)$ $x_{p\_3} := \dfrac{D_{coupling}}{2} \cdot \sin(\theta_3)$

$x_{p\_1} = 0\,mm$ $x_{p\_2} = -112.5833\,mm$ $x_{p\_3} = 112.5833\,mm$

$y_{p\_1} := \dfrac{D_{coupling}}{2} \cdot \cos(\theta_1)$ $y_{p\_2} := \dfrac{D_{coupling}}{2} \cdot \cos(\theta_2)$ $y_{p\_3} := \dfrac{D_{coupling}}{2} \cdot \cos(\theta_3)$

$y_{p\_1} = 130\,mm$ $y_{p\_2} = -65\,mm$ $y_{p\_3} = -65\,mm$

$z_{p\_1} := 2D_{eq\_b\_1}$ $z_{p\_2} := 2D_{eq\_b\_2}$ $z_{p\_3} := 2D_{eq\_b\_3}$

$z_{p\_1} = 60\,mm$ $z_{p\_2} = 60\,mm$ $z_{p\_3} = 60\,mm$

Disturbance Forces:

If multiple forces and moments are applied to the coupling, simple statics should be used to combine load cases to a uniform set of forces and moments applied at a known location (x_L, y_L, z_L).

$x_L := 0mm$ $F_{Lx} := 0N$ $M_{Lx} := 0N \cdot m$

$y_L := 0mm$ $F_{Ly} := -1000 \cos(45deg)\,N$ $M_{Ly} := 0N \cdot m$

$z_L := 0mm$ $F_{Lz} := 1000 \cdot \sin(45 \cdot deg) \cdot N$ $M_{Lz} := 0N \cdot m$

Generalized Geometry of Contact Points Ball to Groove Interface

Location of one contact point:

$$x_1(D, \theta, L) := \frac{D_{coupling}}{2} \cdot \sin(\theta) + \frac{D}{2} \cdot \cos(\theta) \cdot \cos\left(\frac{L}{2}\right)$$

$$y_1(D, \theta, L) := \frac{D_{coupling}}{2} \cdot \cos(\theta) - \frac{D}{2} \cdot \sin(\theta) \cdot \cos\left(\frac{L}{2}\right)$$

$$z_1(D, \theta, L) := \frac{-D}{2} \cdot \sin\left(\frac{L}{2}\right)$$

Location of other contact point:

$$x_2(D, \theta, L) := \frac{D_{coupling}}{2} \cdot \sin(\theta) - \frac{D}{2} \cdot \cos(\theta) \cdot \cos\left(\frac{L}{2}\right)$$

$$y_2(D, \theta, L) := \frac{D_{coupling}}{2} \cdot \cos(\theta) + \frac{D}{2} \cdot \sin(\theta) \cdot \cos\left(\frac{L}{2}\right)$$

$$z_2(D, \theta, L) := \frac{-D}{2} \cdot \sin\left(\frac{L}{2}\right)$$

Equations for Direction Cosines:

$$\alpha(D, \theta, L) := \frac{-\left(\frac{D}{2} \cdot \cos(\theta) \cdot \cos\left(\frac{L}{2}\right)\right)}{\sqrt{\left(\frac{D}{2} \cdot \cos(\theta) \cdot \cos\left(\frac{L}{2}\right)\right)^2 + \left(\frac{D}{2} \cdot \sin(\theta) \cdot \cos\left(\frac{L}{2}\right)\right)^2 + \left(\frac{D}{2} \cdot \sin\left(\frac{L}{2}\right)\right)^2}}$$

$$\beta(D, \theta, L) := \frac{\left(\frac{D}{2} \cdot \sin(\theta) \cdot \cos\left(\frac{L}{2}\right)\right)}{\sqrt{\left(\frac{D}{2} \cdot \cos(\theta) \cdot \cos\left(\frac{L}{2}\right)\right)^2 + \left(\frac{D}{2} \cdot \sin(\theta) \cdot \cos\left(\frac{L}{2}\right)\right)^2 + \left(\frac{D}{2} \cdot \sin\left(\frac{L}{2}\right)\right)^2}}$$

$$\gamma(D, \theta, L) := \frac{\frac{D}{2} \cdot \sin\left(\frac{L}{2}\right)}{\sqrt{\left(\frac{D}{2} \cdot \cos(\theta) \cdot \cos\left(\frac{L}{2}\right)\right)^2 + \left(\frac{D}{2} \cdot \sin(\theta) \cdot \cos\left(\frac{L}{2}\right)\right)^2 + \left(\frac{D}{2} \cdot \sin\left(\frac{L}{2}\right)\right)^2}}$$

Geometry of Contact Points on First Groove

$x_A := x_1(D_{eq\_b\_1}, \theta_1, groove1)$

$x_A = 10.6066\,mm$

$y_A := y_1(D_{eq\_b\_1}, \theta_1, groove1)$

$y_A = 130\,mm$

$z_A := z_1(D_{eq\_b\_1}, \theta_1, groove1)$

$z_A = -10.6066\,mm$

$x_B := x_2(D_{eq\_b\_1}, \theta_1, groove1)$

$x_B = -10.6066\,mm$

$y_B := y_2(D_{eq\_b\_1}, \theta_1, groove1)$

$y_B = 130\,mm$

$z_B := z_2(D_{eq\_b\_1}, \theta_1, groove1)$

$z_B = -10.6066\,mm$

$\alpha_A := \alpha(D_{eq\_b\_1}, \theta_1, groove1)$

$\alpha_A = -0.70711$

$\beta_A := \beta(D_{eq\_b\_1}, \theta_1, groove1)$

$\beta_A = 0$

$\gamma_A := \gamma(D_{eq\_b\_1}, \theta_1, groove1)$

$\gamma_A = 0.70711$

$\alpha_B := -\alpha(D_{eq\_b\_1}, \theta_1, groove1)$

$\alpha_B = 0.70711$

$\beta_B := -\beta(D_{eq\_b\_1}, \theta_1, groove1)$

$\beta_B = 0$

$\gamma_B := \gamma(D_{eq\_b\_1}, \theta_1, groove1)$

$\gamma_B = 0.70711$

Geometry of Contact Points on Second Groove

$x_C := x_1(D_{eq\_b\_2}, \theta_2, groove2)$

$x_C = -117.8866\,mm$

$y_C := y_1(D_{eq\_b\_2}, \theta_2, groove2)$

$y_C = -55.81441\,mm$

$z_C := z_1(D_{eq\_b\_2}, \theta_2, groove2)$

$z_C = -10.6066\,mm$

$x_D := x_2(D_{eq\_b\_2}, \theta_2, groove2)$

$x_D = -107.28\,mm$

$y_D := y_2(D_{eq\_b\_2}, \theta_2, groove2)$

$y_D = -74.18559\,mm$

$z_D := z_2(D_{eq\_b\_2}, \theta_2, groove2)$

$z_D = -10.6066\,mm$

$\alpha_C := \alpha(D_{eq\_b\_2}, \theta_2, groove2)$

$\alpha_C = 0.35355$

$\beta_C := \beta(D_{eq\_b\_2}, \theta_2, groove2)$

$\beta_C = -0.61237$

$\gamma_C := \gamma(D_{eq\_b\_2}, \theta_2, groove2)$

$\gamma_C = 0.70711$

$\alpha_D := -\alpha(D_{eq\_b\_2}, \theta_2, groove2)$

$\alpha_D = -0.35355$

$\beta_D := -\beta(D_{eq\_b\_2}, \theta_2, groove2)$

$\beta_D = 0.61237$

$\gamma_D := \gamma(D_{eq\_b\_2}, \theta_2, groove2)$

$\gamma_D = 0.70711$

Geometry of Contact Points on Third Groove

$x_E := x_1(D_{eq\_b\_3}, \theta_3, groove3)$

$x_E = 107.28\,mm$

$y_E := y_1(D_{eq\_b\_3}, \theta_3, groove3)$

$y_E = -74.18559\,mm$

$z_E := z_1(D_{eq\_b\_3}, \theta_3, groove3)$

$z_E = -10.6066\,mm$

$x_F := x_2(D_{eq\_b\_3}, \theta_3, groove3)$

$x_F = 117.8866\,mm$

$y_F := y_2(D_{eq\_b\_3}, \theta_3, groove3)$

$y_F = -55.81441\,mm$

$z_F := z_2(D_{eq\_b\_3}, \theta_3, groove3)$

$z_F = -10.6066\,mm$

$\alpha_E := \alpha(D_{eq\_b\_3}, \theta_3, groove3)$

$\alpha_E = 0.35355$

$\beta_E := \beta(D_{eq\_b\_3}, \theta_3, groove3)$

$\beta_E = 0.61237$

$\gamma_E := \gamma(D_{eq\_b\_3}, \theta_3, groove3)$

$\gamma_E = 0.70711$

$\alpha_F := -\alpha(D_{eq\_b\_3}, \theta_3, groove3)$

$\alpha_F = -0.35355$

$\beta_F := -\beta(D_{eq\_b\_3}, \theta_3, groove3)$

$\beta_F = -0.61237$

$\gamma_F := \gamma(D_{eq\_b\_3}, \theta_3, groove3)$

$\gamma_F = 0.70711$

Equivalent Radius and Modulus

$$E_1 := \left(\frac{1 - \upsilon_{g1}^2}{E_{g1}} + \frac{1 - \upsilon_{b1}^2}{E_{b1}} \right)^{-1}$$

$E_1 = 1.12894 \times 10^{11} \, Pa$

$$R_1 := \left(\frac{1}{R_{g\_1}} + \frac{1}{R_{b\_maj\_1}} + \frac{1}{R_{b\_min\_1}} \right)^{-1}$$

$R_1 = 0.125 m$

$$E_2 := \left(\frac{1 - \upsilon_{g2}^2}{E_{g2}} + \frac{1 - \upsilon_{b2}^2}{E_{b2}} \right)^{-1}$$

$E_2 = 1.12894 \times 10^{11} \, Pa$

$$R_2 := \left(\frac{1}{R_{g\_2}} + \frac{1}{R_{b\_maj\_2}} + \frac{1}{R_{b\_min\_2}} \right)^{-1}$$

$R_2 = 0.125 m$

$$E_3 := \left(\frac{1 - \upsilon_{g3}^2}{E_{g3}} + \frac{1 - \upsilon_{b3}^2}{E_{b3}} \right)^{-1}$$

$E_3 = 1.12894 \times 10^{11} \, Pa$

$$R_3 := \left(\frac{1}{R_{g\_3}} + \frac{1}{R_{b\_maj\_3}} + \frac{1}{R_{b\_min\_3}} \right)^{-1}$$

$R_3 = 0.125 m$

Miscellaneous Constant for Elliptical Integral Solutions to Hertz Contact Stress Solutions:

$$cos\theta_1 := R_1 \cdot \left[\left(\frac{1}{R_{g\_1}} \right)^2 + \left(\frac{1}{R_{b\_maj\_1}} + 2 \cdot \frac{-1}{R_{g\_1}} - \frac{1}{R_{b\_min\_1}} \right) \right]^{.5} \cdot costheta$$

$cos\theta_1 = 1.25 \times 10^{-7}$

$$cos\theta_2 := R_2 \cdot \left[\left(\frac{1}{R_{g\_2}} \right)^2 + \left(\frac{1}{R_{b\_maj\_2}} + 2 \cdot \frac{-1}{R_{g\_2}} - \frac{1}{R_{b\_min\_2}} \right) \right]^{.5} \cdot costheta$$

$cos\theta_2 = 1.25 \times 10^{-7}$

$$cos\theta_3 := R_3 \cdot \left[\left(\frac{1}{R_{g\_3}} \right)^2 + \left(\frac{1}{R_{b\_maj\_3}} + 2 \cdot \frac{-1}{R_{g\_3}} - \frac{1}{R_{b\_min\_3}} \right) \right]^{.5} \cdot costheta$$

$cos\theta_3 = 1.25 \times 10^{-7}$

$\theta_{11} := acos(cos\theta_1)$ $\theta_{22} := acos(cos\theta_2)$ $\theta_{33} := acos(cos\theta_3)$

$\theta_{11} = 1.5708$ $\theta_{22} = 1.5708$ $\theta_{33} = 1.5708$

$\alpha(\theta) := 1.939 \cdot 2.71831^{-5.26 \cdot \theta} + 1.78 \cdot 2.71831^{-1.09 \cdot \theta} + \frac{.723}{\theta} + .221$

$\beta(\theta) := 35.228 \cdot 2.71831^{-.98 \cdot \theta} - 32.424 \cdot 2.71831^{-1.0475\theta} + 1.486 \cdot \theta - 2.634$

$\lambda(\theta) := -0.214 \cdot 2.71831^{-4.95\theta} - 0.179 \cdot \theta^2 + 0.555\theta + 0.319$

$\alpha_1 := \alpha(\theta_{11})$ $\alpha_2 := \alpha(\theta_{22})$ $\alpha_3 := \alpha(\theta_{33})$

$\alpha_1 = 1.00301$ $\alpha_2 = 1.00301$ $\alpha_3 = 1.00301$

$\beta_1 := \beta(\theta_{11})$ $\beta_2 := \beta(\theta_{22})$ $\beta_3 := \beta(\theta_{33})$

$\beta_1 = 1.00141$ $\beta_2 = 1.00141$ $\beta_3 = 1.00141$

$\lambda_1 := \lambda(\theta_{11})$ $\lambda_2 := \lambda(\theta_{22})$ $\lambda_3 := \lambda(\theta_{33})$

$\lambda_1 = 0.74904$ $\lambda_2 = 0.74904$ $\lambda_3 = 0.74904$

Construction of Position and Force Matrices:

Position Matrix A:

$$A := \begin{pmatrix} \alpha_A \cdot m & \alpha_B \cdot m & \alpha_C \cdot m & \alpha_D \cdot m & \alpha_E \cdot m & \alpha_F \cdot m \\ \beta_A \cdot m & \beta_B \cdot m & \beta_C \cdot m & \beta_D \cdot m & \beta_E \cdot m & \beta_F \cdot m \\ \gamma_A \cdot m & \gamma_B \cdot m & \gamma_C \cdot m & \gamma_D \cdot m & \gamma_E \cdot m & \gamma_F \cdot m \\ -\beta_A \cdot z_A + \gamma_A \cdot y_A & -\beta_B \cdot z_B + \gamma_B \cdot y_B & -\beta_C \cdot z_C + \gamma_C \cdot y_C & -\beta_D \cdot z_D + \gamma_D \cdot y_D & -\beta_E \cdot z_E + \gamma_E \cdot y_E & -\beta_F \cdot z_F + \gamma_F \cdot y_F \\ \alpha_A \cdot z_A - \gamma_A \cdot x_A & \alpha_B \cdot z_B - \gamma_B \cdot x_B & \alpha_C \cdot z_C - \gamma_C \cdot x_C & \alpha_D \cdot z_D - \gamma_D \cdot x_D & \alpha_E \cdot z_E - \gamma_E \cdot x_E & \alpha_F \cdot z_F - \gamma_F \cdot x_F \\ -\alpha_A \cdot y_A + \beta_A \cdot x_A & -\alpha_B \cdot y_B + \beta_B \cdot x_B & -\alpha_C \cdot y_C + \beta_C \cdot x_C & -\alpha_D \cdot y_D + \beta_D \cdot x_D & -\alpha_E \cdot y_E + \beta_E \cdot x_E & -\alpha_F \cdot y_F + \beta_F \cdot x_F \end{pmatrix}$$

$$A = \begin{pmatrix} -0.70711 & 0.70711 & 0.35355 & -0.35355 & 0.35355 & -0.35355 \\ 0 & 0 & -0.61237 & 0.61237 & 0.61237 & -0.61237 \\ 0.70711 & 0.70711 & 0.70711 & 0.70711 & 0.70711 & 0.70711 \\ 0.09192 & 0.09192 & -0.04596 & -0.04596 & -0.04596 & -0.04596 \\ 0 & 0 & 0.07961 & 0.07961 & -0.07961 & -0.07961 \\ 0.09192 & -0.09192 & -0.09192 & 0.09192 & 0.09192 & -0.09192 \end{pmatrix} m$$

Load Matrix B, with and without Disturbance Loads:

$$B_{loads} := \begin{pmatrix} -(F_{px\_1} + F_{px\_2} + F_{px\_3} + F_{Lx}) \cdot 1m \\ -(F_{py\_1} + F_{py\_2} + F_{py\_3} + F_{Ly}) \cdot 1m \\ -(F_{pz\_1} + F_{pz\_2} + F_{pz\_3} + F_{Lz}) \cdot 1m \\ -(-F_{py\_1} \cdot z_{p\_1} - F_{py\_2} \cdot z_{p\_2} - F_{py\_3} \cdot z_{p\_3} + F_{pz\_1} \cdot y_{p\_1} + F_{pz\_2} \cdot y_{p\_2} + F_{pz\_3} \cdot y_{p\_3} - F_{Ly} \cdot z_L + F_{Lz} \cdot y_L + M_{Lx}) \\ -(F_{px\_1} \cdot z_{p\_1} + F_{px\_2} \cdot z_{p\_2} + F_{px\_3} \cdot z_{p\_3} - F_{pz\_1} \cdot x_{p\_1} - F_{pz\_2} \cdot x_{p\_2} - F_{pz\_3} \cdot x_{p\_3} + F_{Lx} \cdot z_L - F_{Lz} \cdot x_L + M_{Ly}) \\ -(F_{px\_1} \cdot y_{p\_1} - F_{px\_2} \cdot y_{p\_2} - F_{px\_3} \cdot y_{p\_3} + F_{py\_1} \cdot x_{p\_1} + F_{py\_2} \cdot x_{p\_2} + F_{py\_3} \cdot x_{p\_3} - F_{Lx} \cdot y_L + F_{Ly} \cdot x_L + M_{Lz}) \end{pmatrix}$$

$$B_{loads} = \begin{pmatrix} 0 \\ 707.10678 \\ 2.92929 \times 10^4 \\ 2.27374 \times 10^{-13} \\ 2.27374 \times 10^{-13} \\ 0 \end{pmatrix} N \cdot m$$

$$B_{noload} := \begin{pmatrix} -(F_{px\_1} + F_{px\_2} + F_{px\_3}) \cdot 1m \\ -(F_{py\_1} + F_{py\_2} + F_{py\_3}) \cdot 1m \\ -(F_{pz\_1} + F_{pz\_2} + F_{pz\_3}) \cdot 1m \\ -(-F_{py\_1} \cdot z_{p\_1} - F_{py\_2} \cdot z_{p\_2} - F_{py\_3} \cdot z_{p\_3} + F_{pz\_1} \cdot y_{p\_1} + F_{pz\_2} \cdot y_{p\_2} + F_{pz\_3} \cdot y_{p\_3}) \\ -(F_{px\_1} \cdot z_{p\_1} + F_{px\_2} \cdot z_{p\_2} + F_{px\_3} \cdot z_{p\_3} - F_{pz\_1} \cdot x_{p\_1} - F_{pz\_2} \cdot x_{p\_2} - F_{pz\_3} \cdot x_{p\_3}) \\ -(F_{px\_1} \cdot y_{p\_1} - F_{px\_2} \cdot y_{p\_2} - F_{px\_3} \cdot y_{p\_3} + F_{py\_1} \cdot x_{p\_1} + F_{py\_2} \cdot x_{p\_2} + F_{py\_3} \cdot x_{p\_3}) \end{pmatrix}$$

$$B_{noload} = \begin{pmatrix} 0 \\ 0 \\ 3 \times 10^4 \\ 2.27374 \times 10^{-13} \\ 2.27374 \times 10^{-13} \\ 0 \end{pmatrix} N \cdot m$$

Solve for Load Matrices:

$$F_{loads} := A^{-1} \cdot B_{loads}$$

$$F_{loads} = \begin{pmatrix} 6.9044 \times 10^3 \\ 6.9044 \times 10^3 \\ 6.6157 \times 10^3 \\ 7.1931 \times 10^3 \\ 7.1931 \times 10^3 \\ 6.6157 \times 10^3 \end{pmatrix} N$$

$$F_{noload} := A^{-1} \cdot B_{noload}$$

$$F_{noload} = \begin{pmatrix} 7.0711 \times 10^3 \\ 7.0711 \times 10^3 \\ 7.0711 \times 10^3 \\ 7.0711 \times 10^3 \\ 7.0711 \times 10^3 \\ 7.0711 \times 10^3 \end{pmatrix} N$$

Determine Coordinates of Balls in Original State and with Deflections cause by Hertz Deformation:

Original Ball Coordinates

$$x_{O\_1} := \frac{x_A + x_B + D_{eq\_b\_1} \cdot \alpha_A + D_{eq\_b\_1} \cdot \alpha_B}{2}$$

$$y_{O\_1} := \frac{y_A + y_B + D_{eq\_b\_1} \cdot \beta_A + D_{eq\_b\_1} \cdot \beta_B}{2}$$

$$z_{O\_1} := \frac{z_A + z_B + .5 D_{eq\_b\_1} \cdot \gamma_A + .5 D_{eq\_b\_1} \cdot \gamma_B}{2}$$

$$x_{O\_1} = 0\,m$$

$$y_{O\_1} = 0.13\,m$$

$$z_{O\_1} = 0\,m$$

$$x_{O\_2} := \frac{x_C + x_D + D_{eq\_b\_2} \cdot \alpha_C + D_{eq\_b\_2} \cdot \alpha_D}{2}$$

$$y_{O\_2} := \frac{y_C + y_D + D_{eq\_b\_2} \cdot \beta_C + D_{eq\_b\_2} \cdot \beta_D}{2}$$

$$z_{O\_2} := \frac{z_C + z_D + .5 D_{eq\_b\_2} \cdot \gamma_C + .5 D_{eq\_b\_2} \cdot \gamma_D}{2}$$

$$x_{O\_2} = -0.11258\,m$$

$$y_{O\_2} = -0.065\,m$$

$$z_{O\_2} = 0\,m$$

$$x_{O\_3} := \frac{x_E + x_F + D_{eq\_b\_3} \cdot \alpha_E + D_{eq\_b\_3} \cdot \alpha_F}{2}$$

$$y_{O\_3} := \frac{y_E + y_F + D_{eq\_b\_3} \cdot \beta_E + D_{eq\_b\_3} \cdot \beta_F}{2}$$

$$z_{O\_3} := \frac{z_E + z_F + .5 D_{eq\_b\_3} \cdot \gamma_E + .5 D_{eq\_b\_3} \cdot \gamma_F}{2}$$

$$x_{O\_3} = 0.11258\,m$$

$$y_{O\_3} = -0.065\,m$$

$$z_{O\_3} = 0\,m$$

Deflection in to Ball at Each Contact Point:

$$\Delta_A := \lambda_1 \left[\left(\frac{2 \cdot \left(F_{loads_{0,0}}\right)^2}{3 \cdot R_1 \cdot E_1^2}\right)^{\frac{1}{3}} - \lambda_1 \cdot \left(\frac{2 \cdot \left(F_{noload_{0,0}}\right)^2}{3 R_1 \cdot E_1^2}\right)^{\frac{1}{3}} \right]$$

$$\Delta_A = -3.25615 \times 10^{-7} \text{ m}$$

$$\Delta_B := \lambda_1 \left[\left(\frac{2 \cdot \left(F_{loads_{1,0}}\right)^2}{3 \cdot R_1 \cdot E_1^2}\right)^{\frac{1}{3}} - \lambda_1 \cdot \left(\frac{2 \cdot \left(F_{noload_{1,0}}\right)^2}{3 R_1 \cdot E_1^2}\right)^{\frac{1}{3}} \right]$$

$$\Delta_B = -3.25615 \times 10^{-7} \text{ m}$$

$$\Delta_C := \lambda_2 \left[\left(\frac{2 \cdot \left(F_{loads_{2,0}}\right)^2}{3 \cdot R_2 \cdot E_2^2}\right)^{\frac{1}{3}} - \lambda_2 \cdot \left(\frac{2 \cdot \left(F_{noload_{2,0}}\right)^2}{3 R_2 \cdot E_2^2}\right)^{\frac{1}{3}} \right]$$

$$\Delta_C = -8.95872 \times 10^{-7} \text{ m}$$

$$\Delta_D := \lambda_2 \left[\left(\frac{2 \cdot \left(F_{loads_{3,0}}\right)^2}{3 \cdot R_2 \cdot E_2^2}\right)^{\frac{1}{3}} - \lambda_2 \cdot \left(\frac{2 \cdot \left(F_{noload_{3,0}}\right)^2}{3 R_2 \cdot E_2^2}\right)^{\frac{1}{3}} \right]$$

$$\Delta_D = 2.36747 \times 10^{-7} \text{ m}$$

$$\Delta_E := \lambda_3 \left[\left(\frac{2 \cdot \left(F_{loads_{4,0}}\right)^2}{3 \cdot R_3 \cdot E_3^2}\right)^{\frac{1}{3}} - \lambda_3 \cdot \left(\frac{2 \cdot \left(F_{noload_{4,0}}\right)^2}{3 R_3 \cdot E_3^2}\right)^{\frac{1}{3}} \right]$$

$$\Delta_E = 2.36747 \times 10^{-7} \text{ m}$$

$$\Delta_F := \lambda_3 \left[\left(\frac{2 \cdot \left(F_{loads_{5,0}}\right)^2}{3 \cdot R_3 \cdot E_3^2}\right)^{\frac{1}{3}} - \lambda_3 \cdot \left(\frac{2 \cdot \left(F_{noload_{5,0}}\right)^2}{3 R_3 \cdot E_3^2}\right)^{\frac{1}{3}} \right]$$

$$\Delta_F = -8.95872 \times 10^{-7} \text{ m}$$

New Ball Coordinates:

$$x_{N\_1} := x_{O\_1} + \frac{\left(\alpha_A \cdot \Delta_A + \alpha_B \cdot \Delta_B\right)}{2}$$

$$y_{N\_1} := y_{O\_1} + \frac{\left(\beta_A \cdot \Delta_A + \beta_B \cdot \Delta_B\right)}{2}$$

$$z_{N\_1} := z_{O\_1} + \frac{\left(\gamma_A \cdot \Delta_A + \gamma_B \cdot \Delta_B\right)}{2}$$

$$x_{N\_1} = 0 \text{ m}$$
$$y_{N\_1} = 0.13 \text{ m}$$
$$z_{N\_1} = -2.30245 \times 10^{-7} \text{ m}$$

$$x_{N\_2} := x_{O\_2} + \frac{\left(\alpha_C \cdot \Delta_C + \alpha_D \cdot \Delta_D\right)}{2}$$

$$y_{N\_2} := y_{O\_2} + \frac{\left(\beta_C \cdot \Delta_C + \beta_D \cdot \Delta_D\right)}{2}$$

$$z_{N\_2} := z_{O\_2} + \frac{\left(\gamma_C \cdot \Delta_C + \gamma_D \cdot \Delta_D\right)}{2}$$

$$x_{N\_2} = -0.11258 \text{ m}$$
$$y_{N\_2} = -0.065 \text{ m}$$
$$z_{N\_2} = -2.33036 \times 10^{-7} \text{ m}$$

$$x_{N\_3} := x_{O\_3} + \frac{\left(\alpha_E \cdot \Delta_E + \alpha_F \cdot \Delta_F\right)}{2}$$

$$y_{N\_3} := y_{O\_3} + \frac{\left(\beta_E \cdot \Delta_E + \beta_F \cdot \Delta_F\right)}{2}$$

$$z_{N\_3} := z_{O\_3} + \frac{\left(\gamma_E \cdot \Delta_E + \gamma_F \cdot \Delta_F\right)}{2}$$

$$x_{N\_3} = 0.11258 \text{ m}$$
$$y_{N\_3} = -0.065 \text{ m}$$
$$z_{N\_3} = -2.33036 \times 10^{-7} \text{ m}$$

Deflection of Ball Centers:

$$dx_1 := x_{N\_1} - x_{O\_1} \qquad dx_1 = 0 \text{ m}$$
$$dy_1 := y_{N\_1} - y_{O\_1} \qquad dy_1 = 0 \text{ m}$$
$$dz_1 := z_{N\_1} - z_{O\_1} \qquad dz_1 = -2.30245 \times 10^{-7} \text{ m}$$

$$dx_2 := x_{N\_2} - x_{O\_2} \qquad dx_2 = -2.00221 \times 10^{-7} \text{ m}$$
$$dy_2 := y_{N\_2} - y_{O\_2} \qquad dy_2 = 3.46792 \times 10^{-7} \text{ m}$$
$$dz_2 := z_{N\_2} - z_{O\_2} \qquad dz_2 = -2.33036 \times 10^{-7} \text{ m}$$

$$dx_3 := x_{N\_3} - x_{O\_3} \qquad dx_3 = 2.00221 \times 10^{-7} \text{ m}$$
$$dy_3 := y_{N\_3} - y_{O\_3} \qquad dy_3 = 3.46792 \times 10^{-7} \text{ m}$$
$$dz_3 := z_{N\_3} - z_{O\_3} \qquad dz_3 = -2.33036 \times 10^{-7} \text{ m}$$

Theory Applicability Test:

Original distance between balls:

$$L_{12O} := \sqrt{(x_{O\_1} - x_{O\_2})^2 + (y_{O\_1} - y_{O\_2})^2 + (z_{O\_1} - z_{O\_2})^2}$$

$$L_{23O} := \sqrt{(x_{O\_2} - x_{O\_3})^2 + (y_{O\_2} - y_{O\_3})^2 + (z_{O\_2} - z_{O\_3})^2}$$

$$L_{31O} := \sqrt{(x_{O\_3} - x_{O\_1})^2 + (y_{O\_3} - y_{O\_1})^2 + (z_{O\_3} - z_{O\_1})^2}$$

$L_{12O} = 0.22517\,m$ $L_{23O} = 0.22517\,m$ $L_{31O} = 0.22517\,m$

Final distance between balls:

$$L_{12N} := \sqrt{(x_{N\_1} - x_{N\_2})^2 + (y_{N\_1} - y_{N\_2})^2 + (z_{N\_1} - z_{N\_2})^2}$$

$$L_{23N} := \sqrt{(x_{N\_2} - x_{N\_3})^2 + (y_{N\_2} - y_{N\_3})^2 + (z_{N\_2} - z_{N\_3})^2}$$

$$L_{31N} := \sqrt{(x_{N\_3} - x_{N\_1})^2 + (y_{N\_3} - y_{N\_1})^2 + (z_{N\_3} - z_{N\_1})^2}$$

$L_{12N} = 0.22517\,m$ $L_{23N} = 0.22517\,m$ $L_{31N} = 0.22517\,m$

Difference between initial and final distances:

$DL_{12} := L_{12O} - L_{12N}$

$DL_{23} := L_{23O} - L_{23N}$

$DL_{31} := L_{31O} - L_{31N}$

$DL_{12} = 2.0022 \times 10^{-7}\,m$

$DL_{23} = -4.00441 \times 10^{-7}\,m$

$DL_{31} = 2.0022 \times 10^{-7}\,m$

Change in length divided by initial distance between balls:

$$D_{12} := \left|\frac{DL_{12}}{L_{12O}}\right|$$

$$D_{23} := \left|\frac{DL_{23}}{L_{23O}}\right|$$

$$D_{31} := \left|\frac{DL_{31}}{L_{31O}}\right|$$

$D_{12} = 8.8921 \times 10^{-7}$

$D_{23} = 1.77842 \times 10^{-6}$

$D_{31} = 8.8921 \times 10^{-7}$

Deflection divided by ball radius:

$$defl_1 := \frac{max\left(|\Delta_A| \cdot |\Delta_B|\right)}{\dfrac{D_{eq\_b\_1}}{2}}$$

$$defl_2 := \frac{max\left(|\Delta_C| \cdot |\Delta_D|\right)}{\dfrac{D_{eq\_b\_2}}{2}}$$

$$defl_3 := \frac{max\left(|\Delta_E| \cdot |\Delta_F|\right)}{\dfrac{D_{eq\_b\_3}}{2}}$$

$defl_1 = 2.17077 \times 10^{-5}$

$defl_2 = 5.97248 \times 10^{-5}$

$defl_3 = 5.97248 \times 10^{-5}$

Ratio (should be greater than 5):

$$Ratio_{12} := \frac{defl_1}{D_{12}}$$

$$Ratio_{23} := \frac{defl_2}{D_{23}}$$

$$Ratio_{31} := \frac{defl_3}{D_{31}}$$

$Ratio_{12} = 24.41233$

$Ratio_{23} = 33.58304$

$Ratio_{31} = 67.16616$

Developing Error Matrices:

Original angles between balls:

$$Ang1 := acos\left(\frac{L_{23O}^2 - L_{12O}^2 - L_{31O}^2}{-2 \cdot L_{12O} \cdot L_{31O}}\right)$$

$$Ang1 = 60 \, deg$$

$$Ang2 := acos\left(\frac{L_{31O}^2 - L_{12O}^2 - L_{23O}^2}{-2 \cdot L_{12O} \cdot L_{23O}}\right)$$

$$Ang2 = 60 \, deg$$

$$Ang3 := acos\left(\frac{L_{12O}^2 - L_{31O}^2 - L_{23O}^2}{-2 \cdot L_{31O} \cdot L_{23O}}\right)$$

$$Ang3 = 60 \, deg$$

Original angles of sides with x-axis:

$$Ang12 := atan2(x_{O\_1} - x_{O\_2}, y_{O\_1} - y_{O\_2})$$

$$Ang12 = 60 \, deg$$

$$Ang23 := atan2(x_{O\_3} - x_{O\_2}, y_{O\_3} - y_{O\_2})$$

$$Ang23 = -2.1188 \times 10^{-14} \, deg$$

$$Ang31 := atan2(x_{O\_1} - x_{O\_3}, y_{O\_1} - y_{O\_3})$$

$$Ang31 = 120 \, deg$$

Original altitude lengths:

$$A_1 := L_{12N} \cdot sin\left(\left|Ang12 - Ang23\right|\right)$$

$$A_1 = 0.195 \, m$$

$$A_2 := L_{23N} \cdot sin\left(\left|Ang12 - Ang23\right|\right)$$

$$A_2 = 0.195 \, m$$

$$A_3 := L_{23N} \cdot sin\left(\left|Ang31 - Ang23\right|\right)$$

$$A_3 = 0.195 \, m$$

New angles between balls:

$$Ang1N := acos\left(\frac{L_{23N}^2 - L_{12N}^2 - L_{31N}^2}{-2 \cdot L_{12N} \cdot L_{31N}}\right)$$

$$Ang1N = 60.00018 \, deg$$

$$Ang2N := acos\left(\frac{L_{31N}^2 - L_{12N}^2 - L_{23N}^2}{-2 \cdot L_{12N} \cdot L_{23N}}\right)$$

$$Ang2N = 59.99991 \, deg$$

$$Ang3N := acos\left(\frac{L_{12N}^2 - L_{31N}^2 - L_{23N}^2}{-2 \cdot L_{31N} \cdot L_{23N}}\right)$$

$$Ang3N = 59.99991 \, deg$$

New angles of sides with x-axis:

$$Ang12N := atan2(x_{N\_1} - x_{N\_2}, y_{N\_1} - y_{N\_2})$$

$$Ang12N = 59.99991 \, deg$$

$$Ang23N := atan2(x_{N\_3} - x_{N\_2}, y_{N\_3} - y_{N\_2})$$

$$Ang23N = -2.1188 \times 10^{-14} \, deg$$

$$Ang31N := atan2(x_{N\_1} - x_{N\_3}, y_{N\_1} - y_{N\_3})$$

$$Ang31N = 120.00009 \, deg$$

Original altitudes slope angles and y-intercepts:

$$slope_2 := Ang23 + \frac{Ang2}{2}$$

$$slope_2 = 30 \, deg$$

$$slope_3 := Ang31 + \frac{Ang3}{2}$$

$$slope_3 = 150 \, deg$$

$$b_2 := y_{O\_2} - tan(slope_2) \cdot x_{O\_2}$$

$$b_2 = 0 \, m$$

$$b_3 := y_{O\_3} - tan(slope_3) \cdot x_{O\_3}$$

$$b_3 = 0 \, m$$

Initial Centroid:

$$x_{ci} := \frac{b_3 - b_2}{slope_2 - slope_3}$$

$$y_{ci} := slope_2 \cdot x_{ci} + b_2$$

$$z_{ci} := \frac{z_{O\_1} + z_{O\_2} + z_{O\_3}}{3}$$

$$x_{ci} = 0 \, m$$

$$y_{ci} = 0 \, m$$

$$z_{ci} = 0 \, m$$

Distance from each ball to the centroid:

$$D_{centroid1} := \sqrt{(x_{N\_1} - x_{ci})^2 + (y_{N\_1} - y_{ci})^2 + (z_{N\_1} - z_{ci})^2}$$

$$D_{centroid1} = 0.13 m$$

$$D_{centroid2} := \sqrt{(x_{N\_2} - x_{ci})^2 + (y_{N\_2} - y_{ci})^2 + (z_{N\_2} - z_{ci})^2}$$

$$D_{centroid2} = 0.13 m$$

$$D_{centroid3} := \sqrt{(x_{N\_3} - x_{ci})^2 + (y_{N\_3} - y_{ci})^2 + (z_{N\_3} - z_{ci})^2}$$

$$D_{centroid3} = 0.13 m$$

Error motion at centroid from weighted ball motion:

$$d_{xc} := dx_1 \cdot \frac{(L_{12O} - D_{centroid1})}{L_{12O}} + dx_2 \cdot \frac{(L_{23O} - D_{centroid2})}{L_{23O}} + dx_3 \cdot \frac{(L_{31O} - D_{centroid3})}{L_{31O}}$$

$$d_{xc} = 0 m$$

$$d_{yc} := dy_1 \cdot \frac{(L_{12O} - D_{centroid1})}{L_{12O}} + dy_2 \cdot \frac{(L_{23O} - D_{centroid2})}{L_{23O}} + dy_3 \cdot \frac{(L_{31O} - D_{centroid3})}{L_{31O}}$$

$$d_{yc} = 2.93143 \times 10^{-7} m$$

$$d_{zc} := dz_1 \cdot \frac{(L_{12O} - D_{centroid1})}{L_{12O}} + dz_2 \cdot \frac{(L_{23O} - D_{centroid2})}{L_{23O}} + dz_3 \cdot \frac{(L_{31O} - D_{centroid3})}{L_{31O}}$$

$$d_{zc} = -2.94298 \times 10^{-7} m$$

Rotation about side due to z motion of opposite ball:

$$T_{23} := \frac{dz_1}{A_1} \qquad T_{23} = -1.18074 \times 10^{-6} \qquad \text{Rotation about side 23 due to z-motion at ball one}$$

$$T_{31} := \frac{dz_2}{A_2} \qquad T_{31} = -1.19505 \times 10^{-6} \qquad \text{Rotation about side 31 due to z-motion at ball one}$$

$$T_{12} := \frac{dz_3}{A_3} \qquad T_{12} = -1.19505 \times 10^{-6} \qquad \text{Rotation about side 12 due to z-motion at ball one}$$

Coupling Error Rotations:

$$\varepsilon_{z1} := \sqrt{\left[.5\left(\alpha_A \cdot \Delta_A + \alpha_B \cdot \Delta_B\right)\right]^2 + \left[.5\left(\beta_A \cdot \Delta_A + \beta_B \cdot \Delta_B\right)\right]^2} \cdot \frac{\text{sign}\left[-\left(\alpha_A \cdot \Delta_A + \alpha_B \cdot \Delta_B\right)\right]}{\sqrt{\left(x_{O\_1} - x_{ci}\right)^2 + \left(y_{O\_1} - y_{ci}\right)^2}}$$

$$\varepsilon_{z2} := \sqrt{\left[.5\left(\alpha_C \cdot \Delta_C + \alpha_D \cdot \Delta_D\right)\right]^2 + \left[.5\left(\beta_C \cdot \Delta_C + \beta_D \cdot \Delta_D\right)\right]^2} \cdot \frac{\text{sign}\left(\alpha_C \cdot \Delta_C + \alpha_D \cdot \Delta_D\right)}{\sqrt{\left(x_{O\_2} - x_{ci}\right)^2 + \left(y_{O\_2} - y_{ci}\right)^2}}$$

$$\varepsilon_{z3} := \sqrt{\left[.5\left(\alpha_E \cdot \Delta_E + \alpha_F \cdot \Delta_F\right)\right]^2 + \left[.5\left(\beta_E \cdot \Delta_E + \beta_F \cdot \Delta_F\right)\right]^2} \cdot \frac{\text{sign}\left(\alpha_E \cdot \Delta_E + \alpha_F \cdot \Delta_F\right)}{\sqrt{\left(x_{O\_3} - x_{ci}\right)^2 + \left(y_{O\_3} - y_{ci}\right)^2}}$$

$$\varepsilon_x := T_{23} \cdot \cos\left(Ang_{23}\right) + T_{31} \cdot \cos\left(Ang_{31}\right) - T_{12} \cdot \cos\left(Ang_{12}\right)$$

$$\varepsilon_y := T_{23} \cdot \sin\left(Ang_{23}\right) + T_{31} \cdot \sin\left(Ang_{31}\right) - T_{12} \cdot \sin\left(Ang_{12}\right)$$

$$\varepsilon_z := \frac{\varepsilon_{z1} + \varepsilon_{z2} + \varepsilon_{z3}}{3}$$

$$\varepsilon_{z1} = 0$$

$$\varepsilon_{z2} = -3.08032 \times 10^{-6}$$

$$\varepsilon_{z3} = 3.08032 \times 10^{-6}$$

$$\varepsilon_x = 1.43114 \times 10^{-8}$$

$$\varepsilon_y = 0$$

$$\varepsilon_z = 0$$

Coupling Error Motions

Coupling Homogeneous Transformation Matrix:

$$HTM := \begin{pmatrix} 1 & -\epsilon_z & \epsilon_y & \dfrac{d_{xc}}{m} \\ \epsilon_z & 1 & -\epsilon_x & \dfrac{d_{yc}}{m} \\ -\epsilon_y & \epsilon_x & 1 & \dfrac{d_{zc}}{m} \\ 0 & 0 & 0 & 1 \end{pmatrix}$$

$$HTM = \begin{pmatrix} 1 & 0 & 0 & 0 \\ 0 & 1 & 0 & 0 \\ 0 & 1.43114\times10^{-8} & -1.43114\times10^{-8} & 2.93143\times10^{-7} \\ 0 & 0 & -2.94298\times10^{-7} & 1 \end{pmatrix}$$

Point of interest:

$$Point := \begin{pmatrix} x_{err} - x_{ci} \\ y_{err} - y_{ci} \\ z_{err} - z_{ci} \\ 1m \end{pmatrix}$$

$$Point = \begin{pmatrix} -0.25 \\ 0 \\ 0.5 \\ 1 \end{pmatrix} m$$

Error Displacements:

$$\Delta := HTM \cdot Point - Point$$

$$\Delta = \begin{pmatrix} 0 \\ 2.85988\times10^{-7} \\ -2.94298\times10^{-7} \\ 0 \end{pmatrix} m$$

Contact Ellipses

$$R_{major\_A} := \alpha_1 \cdot \left(1.5 \cdot F_{loads_{0,0}} \cdot \frac{R_1}{E_1} \right)^{\frac{1}{3}}$$

$$R_{major\_B} := \alpha_1 \cdot \left(1.5 \cdot F_{loads_{1,0}} \cdot \frac{R_1}{E_1} \right)^{\frac{1}{3}}$$

$$R_{major\_C} := \alpha_2 \cdot \left(1.5 \cdot F_{loads_{2,0}} \cdot \frac{R_2}{E_2} \right)^{\frac{1}{3}}$$

$$R_{major\_D} := \alpha_2 \cdot \left(1.5 \cdot F_{loads_{3,0}} \cdot \frac{R_2}{E_2} \right)^{\frac{1}{3}}$$

$$R_{major\_E} := \alpha_3 \cdot \left(1.5 \cdot F_{loads_{4,0}} \cdot \frac{R_3}{E_3} \right)^{\frac{1}{3}}$$

$$R_{major\_F} := \alpha_3 \cdot \left(1.5 \cdot F_{loads_{5,0}} \cdot \frac{R_3}{E_3} \right)^{\frac{1}{3}}$$

$$R_{minor\_A} := \beta_1 \cdot \left(1.5 \cdot F_{loads_{0,0}} \cdot \frac{R_1}{E_1} \right)^{\frac{1}{3}}$$

$$R_{minor\_B} := \beta_1 \cdot \left(1.5 \cdot F_{loads_{1,0}} \cdot \frac{R_1}{E_1} \right)^{\frac{1}{3}}$$

$$R_{minor\_C} := \beta_2 \cdot \left(1.5 \cdot F_{loads_{2,0}} \cdot \frac{R_2}{E_2} \right)^{\frac{1}{3}}$$

$$R_{minor\_D} := \beta_2 \cdot \left(1.5 \cdot F_{loads_{3,0}} \cdot \frac{R_2}{E_2} \right)^{\frac{1}{3}}$$

$$R_{minor\_E} := \beta_3 \cdot \left(1.5 \cdot F_{loads_{4,0}} \cdot \frac{R_3}{E_3} \right)^{\frac{1}{3}}$$

$$R_{minor\_F} := \beta_3 \cdot \left(1.5 \cdot F_{loads_{5,0}} \cdot \frac{R_3}{E_3} \right)^{\frac{1}{3}}$$

$$R_{major\_A} = 2.26182 \times 10^{-3} \ m \qquad R_{minor\_A} = 2.2582 \times 10^{-3} \ m \qquad R_{minor\_D} = 2.28925 \times 10^{-3} \ m$$

$$R_{major\_B} = 2.26182 \times 10^{-3} \ m \qquad R_{minor\_B} = 2.2582 \times 10^{-3} \ m \qquad R_{minor\_E} = 2.28925 \times 10^{-3} \ m$$

$$R_{major\_C} = 2.22985 \times 10^{-3} \ m \qquad R_{minor\_C} = 2.22628 \times 10^{-3} \ m \qquad R_{minor\_F} = 2.22628 \times 10^{-3} \ m$$

$$R_{major\_D} = 2.29292 \times 10^{-3} \ m$$

$$R_{major\_E} = 2.29292 \times 10^{-3} \ m$$

$$R_{major\_F} = 2.22985 \times 10^{-3} \ m$$

Contact Stress:

$$\sigma_A := \frac{3 \cdot F_{loads_{0,0}}}{2 \cdot \pi \cdot R_{major\_A} \cdot R_{minor\_A}}$$

$$\sigma_B := \frac{3 \cdot F_{loads_{1,0}}}{2 \cdot \pi \cdot R_{major\_B} \cdot R_{minor\_B}}$$

$$\sigma_C := \frac{3 \cdot F_{loads_{2,0}}}{2 \cdot \pi \cdot R_{major\_C} \cdot R_{minor\_C}}$$

$$\sigma_D := \frac{3 \cdot F_{loads_{3,0}}}{2 \cdot \pi \cdot R_{major\_D} \cdot R_{minor\_D}}$$

$$\sigma_E := \frac{3 \cdot F_{loads_{4,0}}}{2 \cdot \pi \cdot R_{major\_E} \cdot R_{minor\_E}}$$

$$\sigma_F := \frac{3 \cdot F_{loads_{5,0}}}{2 \cdot \pi \cdot R_{major\_F} \cdot R_{minor\_F}}$$

$$\sigma_A = 6.45425 \times 10^8 \ Pa \qquad \sigma_C = 6.36301 \times 10^8 \ Pa \qquad \sigma_E = 6.54298 \times 10^8 \ Pa$$

$$\sigma_B = 6.45425 \times 10^8 \ Pa \qquad \sigma_D = 6.54298 \times 10^8 \ Pa \qquad \sigma_F = 6.36301 \times 10^8 \ Pa$$

Contact Stress/Allowable Contact Stress:

$$\frac{\sigma_A}{Hertz_{g1}} = 0.37525 \qquad \frac{\sigma_C}{Hertz_{g2}} = 0.36994 \qquad \frac{\sigma_E}{Hertz_{g3}} = 0.38041$$

$$\frac{\sigma_B}{Hertz_{g1}} = 0.37525 \qquad \frac{\sigma_D}{Hertz_{g2}} = 0.38041 \qquad \frac{\sigma_F}{Hertz_{g3}} = 0.36994$$

RMS Error Motion, Forces, and Stiffness:

$$RMS := \sqrt{(\Delta_{0,0})^2 + (\Delta_{1,0})^2 + (\Delta_{2,0})^2}$$

$$RMS = 4.10366 \times 10^{-7} \, m \qquad RMS = 16.15614 \, \mu in$$

$$F_{RMS} := \sqrt{F_{Lx}^2 + F_{Ly}^2 + F_{Lz}^2}$$

$$F_{RMS} = 1 \times 10^3 \, N$$

$$k_{RMS} := \frac{F_{RMS}}{RMS}$$

$$k_{RMS} = 2.43685 \times 10^9 \, \frac{N}{m}$$

$$k_{RMS} = 13.91476 \, \frac{lbf}{\mu in}$$

$$k_x := \left| \frac{F_{Lx}}{\Delta_{0,0}} \right| \qquad\qquad k_y := \left| \frac{F_{Ly}}{\Delta_{1,0}} \right| \qquad\qquad k_z := \left| \frac{F_{Lz}}{\Delta_{2,0}} \right|$$

$$k_x = 0 \, \frac{N}{m} \qquad\qquad k_y = 2.47251 \times 10^9 \, \frac{N}{m} \qquad\qquad k_z = 2.40269 \times 10^9 \, \frac{N}{m}$$

$$k_x = 0 \, \frac{lbf}{\mu in} \qquad\qquad k_y = 14.11839 \, \frac{lbf}{\mu in} \qquad\qquad k_z = 13.71971 \, \frac{lbf}{\mu in}$$

Appendix B

MATHEMATICS FOR THREE PIN COUPLING

Geometry of Coupling:

Main Diameter of Pin:	$d_{full} := 8mm$
Diameter of Relief Area:	$d_{rel} := 5mm$
Length of Relief Diameter:	$L_{rel} := 60mm$
Length of Force Area:	$L_{force} := 20mm$
Young's Modulus:	$E := 70 \times 10^9 Pa$
Angle for Left Pin:	$\alpha := 30deg$
Angle for Right Pin:	$\beta := 30deg$
Angle for Spring Pin:	$\theta := 30deg$
Distance to Left Pin (mm):	$r_L := 40mm$
Distance to Right Pin (mm):	$r_R := 40mm$
Distance to Spring Pin (mm):	$L_{cp} := 62.5mm$
Coefficient of Friction for Interface:	$\mu := 0.1$

Spring Pin

Anvil Pin

Left Pin

Right Pin

Matching Flange Geometry

Geometry Center

r_{cp}

r_L α β r_R θ

Flange

ANVIL

D_{full}

D_{rel}

PIN

L_{force}

L_{rel}

Interface Plate
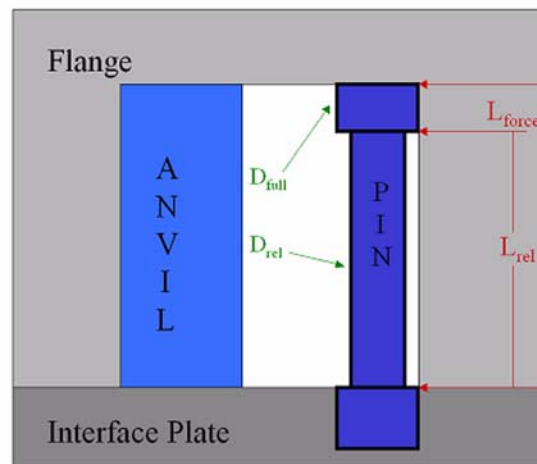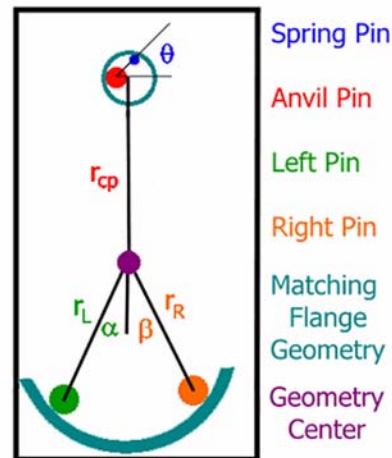
Applied Forces and Moments:

Force in X Direction (N):	$F_x := 0N$
Force in Y Direction (N):	$F_y := 15N$
Force in Z Direction (N):	$F_z := 0N$
Moment in X Direction (N-m):	$M_x := 0N \cdot m$
Moment in Y Direction (N-m):	$M_y := 0N \cdot m$
Moment in Z Direction (N-m):	$M_z := 0N \cdot m$
X Location of Forces (mm):	$x := 0mm$
Y Location of Forces (mm):	$y := 0mm$
Z Location of Forces (mm):	$z := 0mm$
X Rotation of Forces (deg):	$x_{rot} := 0deg$
Y Rotation of Forces (deg):	$y_{rot} := 0deg$
Z Rotation of Forces (deg):	$z_{rot} := 0deg$

Spring Pin

Anvil Pin

Left Pin

Right Pin

Matching Flange Geometry

Geometry Center
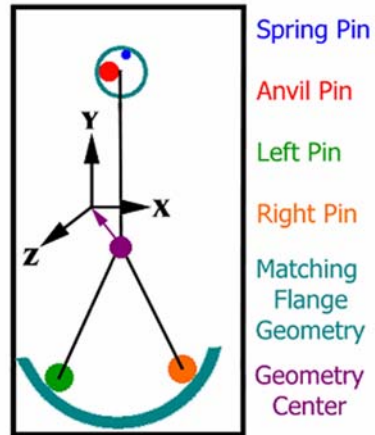
End Displacement of Pin:

$$y := \frac{d_{full} - d_{rel}}{2} \qquad y = 1.5\,mm$$

Moments of Inertia:

$$r_{full} := \frac{d_{full}}{2} \qquad I_{full} := \frac{1}{2} \cdot \pi \cdot r_{full}^4 \qquad I_{full} = 402.124\,mm^4$$

$$r_{rel} := \frac{d_{rel}}{2} \qquad I_{rel} := \frac{1}{2} \cdot \pi \cdot r_{rel}^4 \qquad I_{rel} = 61.359\,mm^4$$

Additional Lengths:

Total External Pin Length: $\qquad L_{pin} := L_{rel} + L_{force} \qquad L_{pin} = 80\,mm$

Length to Force Location on Pin: $\qquad L_f := L_{rel} + \frac{L_{force}}{2} \qquad L_f = 70\,mm$

Force Acting at End of Pin like a Simple Cantilever Beam for Deflection of y:

Forces for Deflections on Pin with Full Diameter:

$$F_{full} := \frac{y \cdot 3 \cdot E \cdot I_{full}}{L_{pin}^3} \qquad F_{full} = 247.4\,N$$

Forces for Deflections on Pin with Relief Diameter:

$$F_{rel} := \frac{y \cdot 3 \cdot E \cdot I_{rel}}{L_{pin}^3} \qquad F_{rel} = 37.75\,N$$

Bending Moment and Stress at Base of Pin:

$$M := F_{rel} \cdot L_f \qquad M = 2.643\,N \cdot m$$

$$\sigma := \frac{M \cdot r_{rel}}{I_{rel}} \qquad \sigma = 107.666 \cdot 10^6\,Pa$$

If more complex pins are used (ie. changing cross section along pin length), then force and deflections must be adjusted to reflect the change. This analysis assumes that the reliefe diameter will bend significantly more than the full diameter at the pin head. Some minor additional deflection will occur along the length of the pin head, but this amount should be less than along the relief. Complete force will be slightly larger than Frel, but significantly smaller than Ffull.

In addition, if spring pin is not used, Frel can be specified to analyze the force summation of a generic three pin coupling.

Determination of total in plane load caused by spring pin preload and frictional resistance:

$$F_{plate} := F_{ml} - \mu \cdot F_z$$

Position Matrix from Summation of Forces and Moments using Free Body Diagram:

$$A :=
\begin{pmatrix}
1m & \sin(\alpha)m & -\sin(\beta)m & 0m & 0m & 0m \\
0m & \cos(\alpha)m & \cos(\beta)m & 0m & 0m & 0m \\
0m & 0m & 0m & 1m & 1m & 1m \\
0m & z\cos(\alpha) & z\cos(\beta) & -(L_{cp}-y) & y + r_L\cos(\alpha) & y + r_R\cos(\beta) \\
-z & -z\sin(\alpha) & z\sin(\beta) & -z & -(z + r_L\sin(\alpha)) & -(z - r_R\sin(\beta)) \\
y - L_{cp} & -z\cos(\alpha) + y\sin(\alpha) & -(z\cos(\beta) + y\sin(\beta)) & 0m & 0m & 0m
\end{pmatrix}$$

$$A =
\begin{pmatrix}
1 & 0.5 & -0.5 & 0 & 0 & 0 \\
0 & 0.866 & 0.866 & 0 & 0 & 0 \\
0 & 0 & 0 & 1 & 1 & 1 \\
0 & 0 & 0 & -0.061 & 0.036 & 0.036 \\
0 & 0 & 0 & 0 & -0.02 & 0.02 \\
-0.061 & 7.5\times10^{-4} & -7.5\times10^{-4} & 0 & 0 & 0
\end{pmatrix} m$$

Force Matrix from Summation of Forces and Moments using Free Body Diagram:

$$V :=
\begin{bmatrix}
[[\cos(z_{rot})\cos(y_{rot})F_x + (\cos(z_{rot})\sin(y_{rot})\sin(x_{rot}) - \sin(z_{rot})\cos(x_{rot}))F_y + (\cos(z_{rot})\sin(y_{rot})\cos(x_{rot}) + \sin(z_{rot})\sin(x_{rot}))F_z] + F_{plate}\cos(\theta)]m \\
[[\sin(z_{rot})\cos(y_{rot})F_x + (\sin(z_{rot})\sin(y_{rot})\sin(x_{rot}) + \cos(z_{rot})\cos(x_{rot}))F_y + (\sin(z_{rot})\sin(y_{rot})\cos(x_{rot}) - \cos(z_{rot})\sin(x_{rot}))F_z] + F_{plate}\sin(\theta)]m \\
(-\sin(y_{rot})F_x + \cos(y_{rot})\sin(x_{rot})F_y + \cos(y_{rot})\cos(x_{rot})F_z)m \\
-[\cos(z_{rot})\cos(y_{rot})M_x - (\cos(z_{rot})\sin(y_{rot})\sin(x_{rot}) - \sin(z_{rot})\cos(x_{rot}))M_y + (\cos(z_{rot})\sin(y_{rot})\cos(x_{rot}) + \sin(z_{rot})\sin(x_{rot}))M_z] - z\sin(\theta)F_{plate} \\
-[\sin(z_{rot})\cos(y_{rot})M_x + (\sin(z_{rot})\sin(y_{rot})\sin(x_{rot}) + \cos(z_{rot})\cos(x_{rot}))M_y + (\sin(z_{rot})\sin(y_{rot})\cos(x_{rot}) - \cos(z_{rot})\sin(x_{rot}))M_z] - z\cos(\theta)F_{plate} \\
-(-\sin(y_{rot})M_x + \cos(y_{rot})\sin(x_{rot})M_y + \cos(y_{rot})\cos(x_{rot})M_z) - (z\sin(\theta) - y\cos(\theta) + L_{cp}\cos(\theta))F_{plate}
\end{bmatrix}$$

$$V =
\begin{pmatrix}
32.693 \\
3.875 \\
0 \\
0 \\
0 \\
-1.994
\end{pmatrix} N\cdot m$$

Solving for forces applied at contact points: $\quad F := \text{lsolve}(A, V)$

Which gives the following forces:

$$F_{anvil} := F_{0,0} \qquad F_{anvil} = 32.693\,N \qquad F_{z\_bolt\_at\_control\_pin} := F_{3,0} \qquad F_{z\_bolt\_at\_control\_pin} = 0\,N$$

$$F_{left} := F_{1,0} \qquad F_{left} = 2.237\,N \qquad F_{z\_bolt\_at\_left\_pin} := F_{4,0} \qquad F_{z\_bolt\_at\_left\_pin} = 0\,N$$

$$F_{right} := F_{2,0} \qquad F_{right} = 2.237\,N \qquad F_{z\_bolt\_at\_right\_pin} := F_{5,0} \qquad F_{z\_bolt\_at\_right\_pin} = 0\,N$$

Appendix C

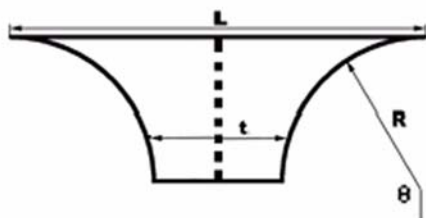## STIFFNESS APPROXIMATIONS FOR FEA OF COUPLING SIMULATION

+ ## *Mathcad Sheet to Find Parameters of CAD Geometry for Equivalent Coupling Stiffness in FEA*
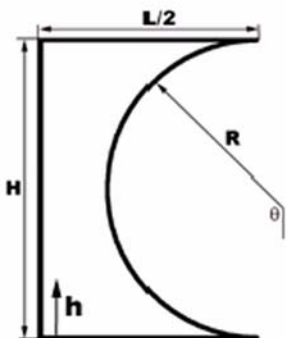
To find compliance or stiffness of subsitute geometry:
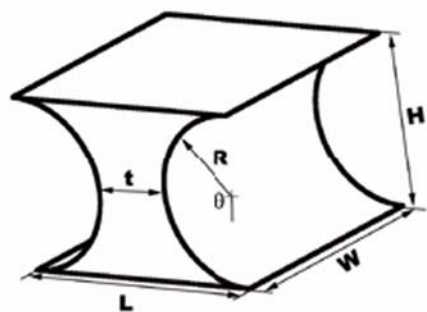
$$k_z = \frac{E \cdot A}{L} = \frac{E \cdot t \cdot W}{H}$$

W and L are constant to size of coupling
H, t, R, and θ are used to get approximated stiffness in z-direction

$$t = L - 2 \cdot R \cdot \sin(\theta)$$

$$R = \frac{H}{2}$$

$$h = \frac{H}{2} \cdot (1 - \cos(\theta))$$

$$h = R(1 - \cos(\theta))$$

Which gives stiffness as a function of θ:

$$k_z(\theta) = \frac{E \cdot (L - 2 \cdot R \cdot \sin(\theta)) \cdot W}{R \cdot (1 - \cos(\theta))}$$

For overall thickness of geometry, integrate over 180 degress:

$$k_z = \int_0^\pi \frac{E \cdot (L - 2 \cdot R \cdot \sin(\theta)) \cdot W}{R \cdot (1 - \cos(\theta))} \, d\theta$$

Since denominator in integral will cause a singularity, invert to find the compliance of the geometry.

$$C_z = \int_0^\pi \frac{R \cdot (1 - \cos(\theta))}{E \cdot (L - 2R \cdot \sin(\theta)) \cdot w} \, d\theta$$

Invert resulting compliance to find stiffness. Repeat until a radius R or height H is found that gives an equivalent stiffness.

Example Calculation:

Input Stiffness from Kinematic Coupling Analysis:

$$k_{KC} := 9.95178 \times 10^7 \frac{N}{m}$$

$$k_{KC\_per\_coupling} := \frac{k_{KC}}{3} \qquad k_{KC\_per\_coupling} = 3.317 \times 10^7 \frac{N}{m}$$

Input Basic Dimensions and Properties of Coupling Material:

$$E := 29.9938 \times 10^6 \, psi$$

$$L := 35mm$$

$$W := 35mm$$

Define equation for coupling stiffness in terms of the height:

$$C_z(h) := \int_0^\pi \frac{\frac{h}{2} \cdot (1 - \cos(\theta))}{E \cdot (L - h \cdot \sin(\theta)) \cdot W} \, d\theta \qquad k_z(h) := \frac{1}{C_z(h)}$$

Iterate to find optimal value of h:

$$h_{opt} := \begin{vmatrix} h_{test} \leftarrow L \\ \text{while } k_z(h_{test}) \leq k_{KC\_per\_coupling} \\ \quad h_{test} \leftarrow h_{test} - .00001 \cdot mm \\ h_{test} \end{vmatrix}$$

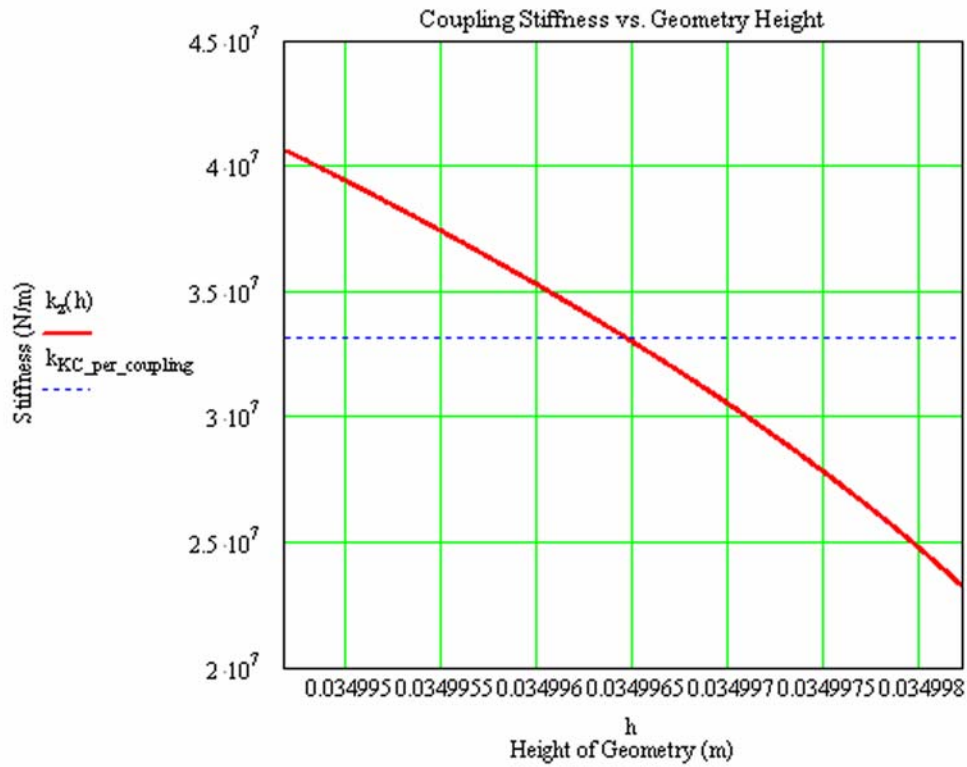$$\boxed{h_{opt} = 34.99645 \, mm}$$
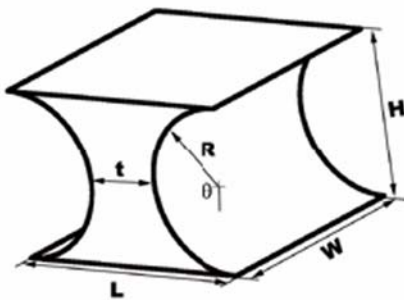
$$\boxed{k_z(h_{opt}) = 3.31815 \times 10^7 \frac{N}{m}}$$

Error of iteration step:

$$error := \frac{k_z(h_{opt}) - k_{KC\_per\_coupling}}{k_{KC\_per\_coupling}}$$

$$\boxed{error = 0.027\%}$$

And a plot of coupling stiffness versus the height of the geometry:

So, final geometric parameters are as follows for a stiffness of $k_z(h_{opt}) = 3.318 \times 10^7 \frac{N}{m}$

$$\boxed{W = 35\,mm}$$

$$\boxed{L = 35\,mm}$$

$$H := h_{opt} \qquad \boxed{H = 34.996\,mm}$$

$$R := \frac{H}{2} \qquad \boxed{R = 17.498\,mm}$$

$$t := L - 2R \qquad \boxed{t = 3.55 \times 10^{-3}\,mm}$$

Equivalent Coupling Stiffness in FEA using Young's Modulus Approximation

$L := 21\,mm$

$K_{kc} := 9.95178 \times 10^7 \dfrac{N}{m}$

$A := 35\,mm \cdot 35\,mm$

$E := \dfrac{L \cdot K_{kc}}{3 \cdot A}$

$E = 5.687 \times 10^8\,Pa$

Appendix D

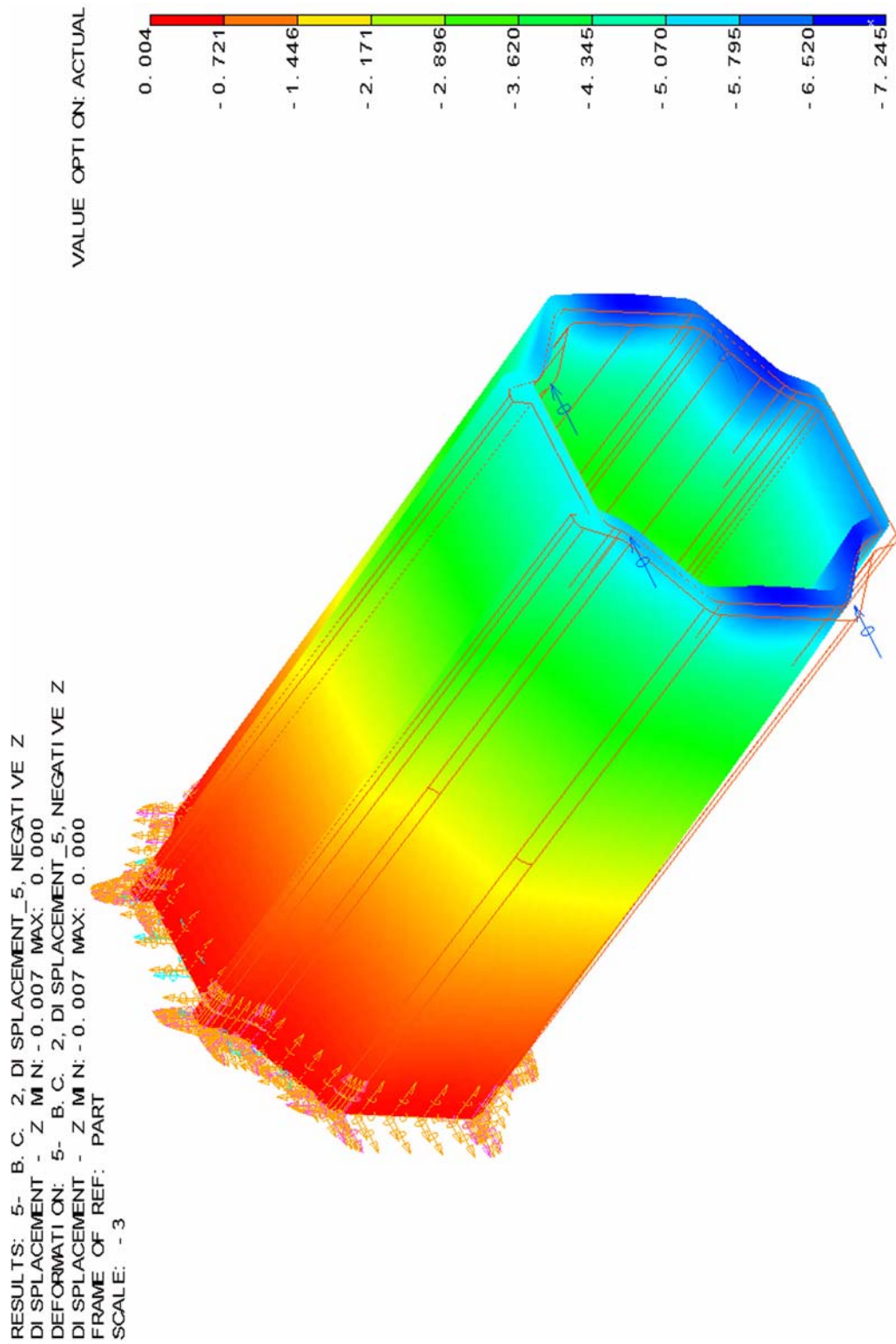## FEA PLOTS FOR WRIST STIFFNESS ANALYSIS
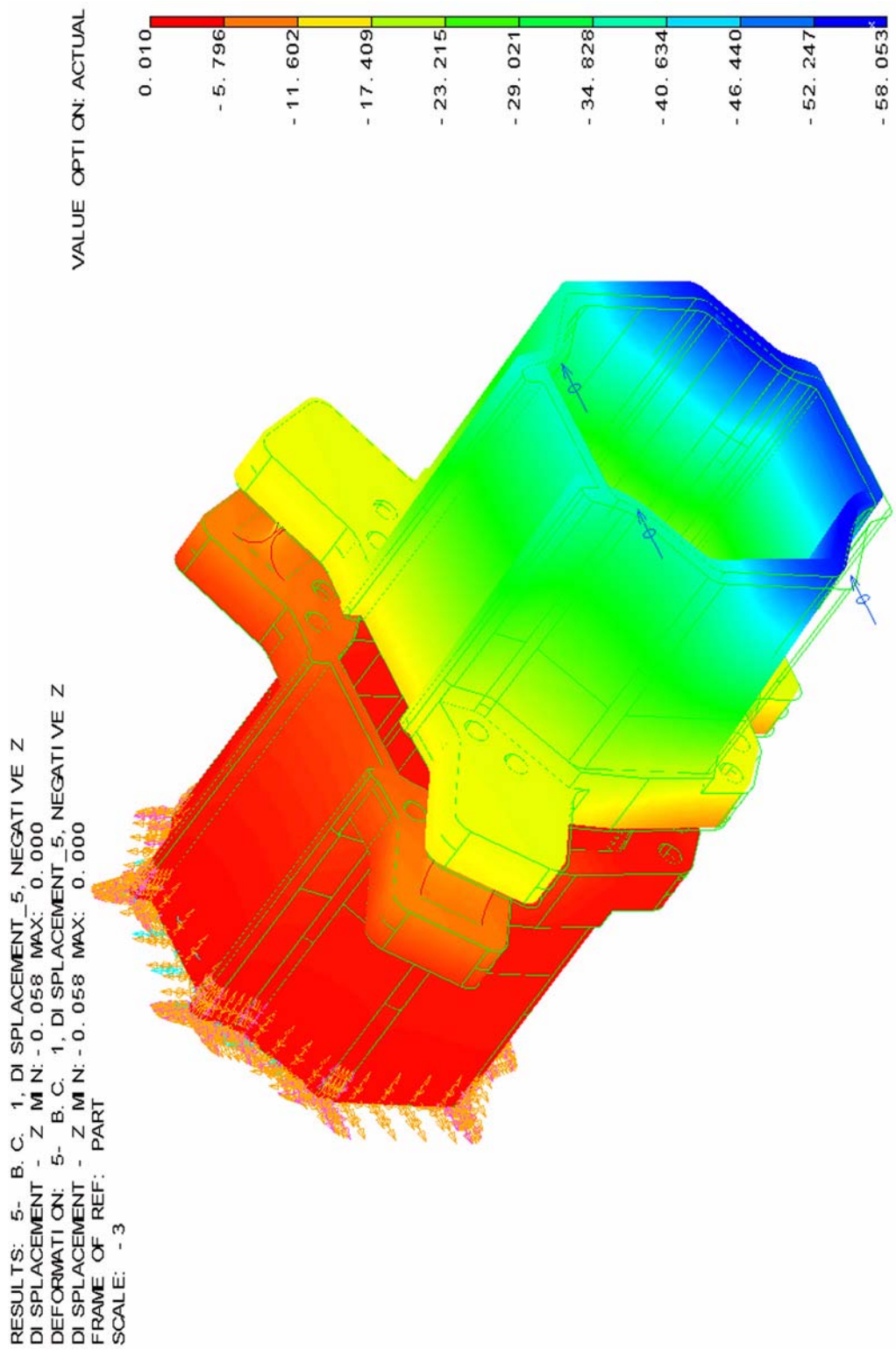
Figure D.1   FEA Results for Straight Beam

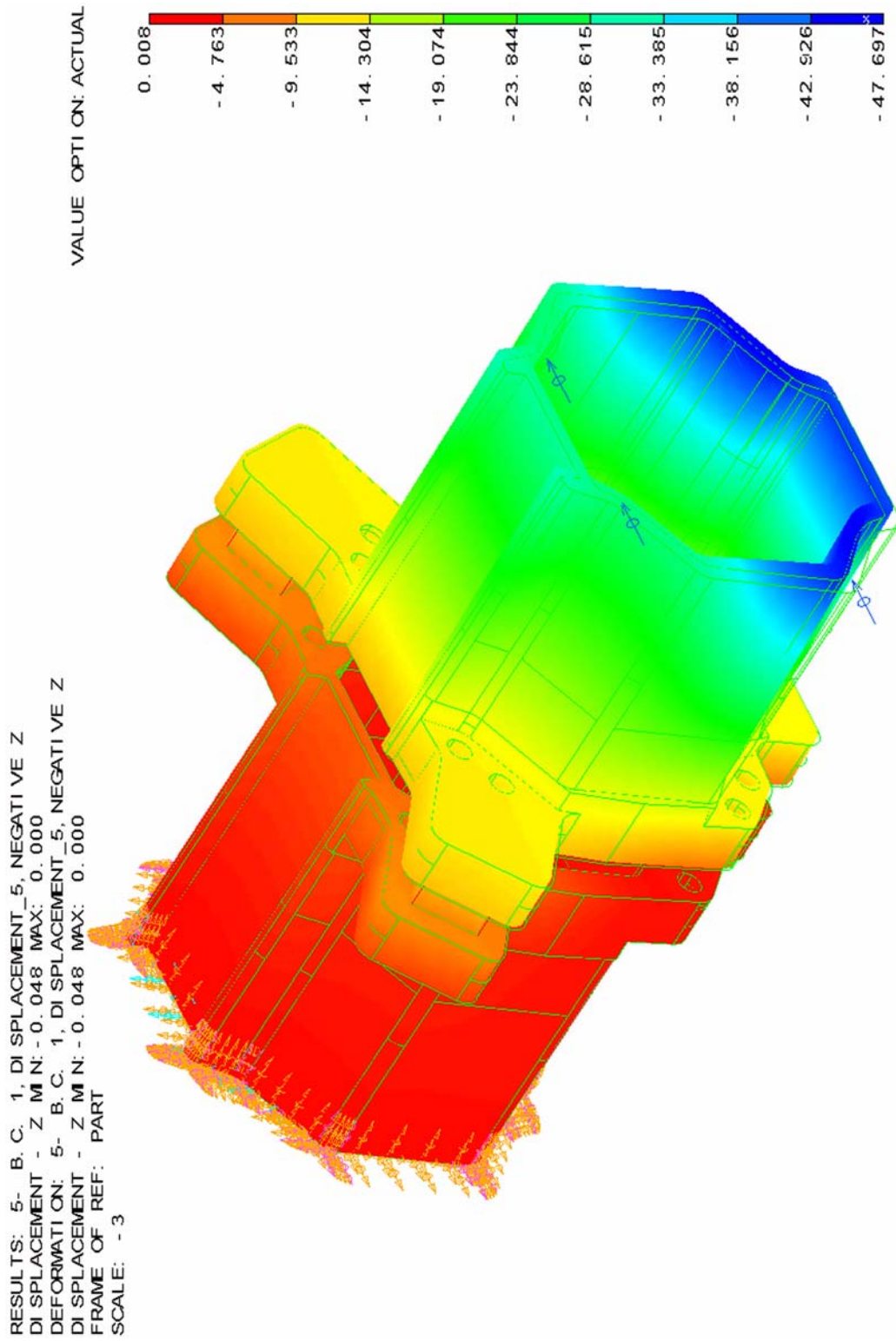**Figure D.2** FEA Results for Canoe Ball Groove Interface with Flexure Approximation

Figure D.3 FEA Results for Canoe Ball Groove Interface with Modulus Approximation